MATERIALS CHEMISTRY FRONTIERS

REVIEW

View Article Online
View Journal | View Issue

Cite this: *Mater. Chem. Front.*, 2020, **4**, 3487

Recent advances in high-performance organic solar cells enabled by acceptor–donor–acceptor–donor–acceptor (A–DA′D–A) type acceptors†‡

Jiajun Zhao,[a] Chao Yao,[a] Muhammad Umair Ali,[ab] Jingsheng Miao*[a] and Hong Meng*[a]

Received 8th May 2020,
Accepted 4th June 2020

DOI: 10.1039/d0qm00305k

rsc.li/frontiers-materials

Over the past two years, the emergence of acceptor–donor–acceptor–donor–acceptor (A–DA′D–A) type non-fullerene acceptors (NFAs) has contributed to the rapid development of organic solar cells (OSCs) with power conversion efficiencies (PCEs) exceeding 18%. In this Minireview, we firstly introduce key factors, including light absorption, energy levels, and morphology of the active layer that affect the performance of OSCs. Then, we spotlight the A–DA′D–A type acceptors for high-efficiency OSCs reported in recent times and summarize the structure–property relationship from selected examples for future molecular design. We also discuss the recent progress in highly efficient ternary OSCs based on A–DA′D–A type acceptors. Finally, we forecast several research directions for further development of OSCs toward commercialization.

1. Introduction

Organic solar cells (OSCs), which directly convert solar resources into electric energy, have been widely recognized as a promising reproducible energy technology owing to their mechanical flexibility, environmental friendliness, and large-scale processability *via* cost-effective methods.[1–7] Since 1995, bulk-heterojunction (BHJ) OSCs have achieved great progress with rapid development in materials synthesis,[8–13] device fabrication,[14–16] and theoretical analysis.[17–19] As an indispensable component of the active layer, electron acceptor materials play a significant role in the photophysical process, and have been dominated by fullerene derivatives for a few decades.[20–22] Nevertheless, fullerene-based acceptors exhibit weak light absorption, restricted chemical structure tunability, and poor device thermal stability, leading to inefficient device performance. To resolve these obstacles, non-fullerene acceptors (NFAs) have emerged as a potential alternative and have been widely investigated. The star NFA molecule, ITIC with an electron push–pull structure, was first

[a] *School of Advanced Materials, Peking University Shenzhen Graduate School, Shenzhen 518055, China. E-mail: menghong@pku.edu.cn, miaojs@pkusz.edu.cn*
[b] *Department of Materials Science and Engineering, College of Engineering, Peking University, Beijing 100871, China*

† Dedicated to Prof. Fred Wudl in celebration of his 80th birthday.

‡ Electronic supplementary information (ESI) available. See DOI: 10.1039/d0qm00305k

Jiajun Zhao

Jiajun Zhao received his BS degree in materials science and engineering from Zhejiang University of Technology (2018). Now he is a master student in the School of Advanced Materials, Peking University Shenzhen Graduate School under the supervision of Prof. Hong Meng. His research interests focus on the design and synthesis of non-fullerene acceptors for organic solar cells.

Chao Yao

Chao Yao is a PhD student under the supervision of Prof. Hong Meng at School of Advanced Materials, Peking University. He received his BS degree in chemistry from Sichuan University in 2014. His research interest focuses on the organic photovoltaic materials.

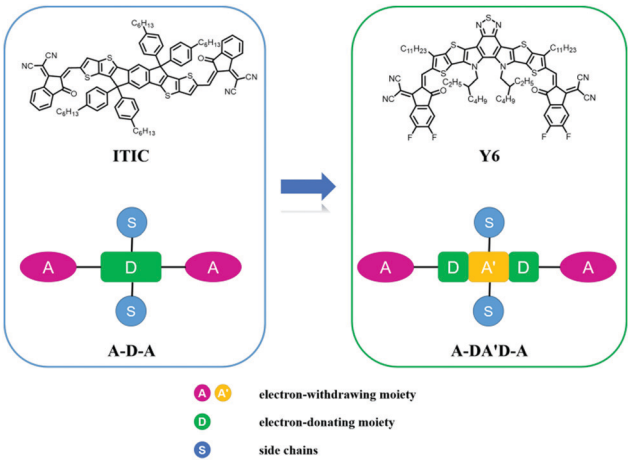

Fig. 1 Chemical structures of ITIC and Y6 and schematic diagrams of A–D–A and A–DA′D–A type acceptors.

reported in 2015 by Zhan *et al.*,[12] and exhibits advantages of facile synthesis, suitable planarity, and easily tunable optoelectronic properties compared with fullerene-based acceptors. As a result, a remarkable power conversion efficiency (PCE) of 6.80% was realized for non-fullerene solar cells at that time. The successful application of ITIC as an excellent NFA reveals great potential of these acceptor–donor–acceptor (A–D–A) type molecules, where the "A" and "D" units represent the electron-withdrawing chromophore and electron-donating aromatically fused rings, respectively (as shown in Fig. 1). Since then, numerous NFAs have been developed and OSCs with record PCEs surpassing 14% have been demonstrated during the past five years.[23–26]

To further improve the efficiency of non-fullerene solar cells, various strategies have been proposed, including ultra-narrow bandgap (UNBG) materials,[27–33] ternary solar cells,[34–38] and tandem solar cells.[39–42] Recently, by strengthening the intramolecular electron push–pull effects, Zou's group constructed a novel A–DA′D–A type acceptor with UNBG, referred to as Y6.[43] The expanded absorption of Y6 near 950 nm enabled remarkably improved current of the corresponding solar cells and the highest PCE of 15.7% has been attained, significantly outperforming the ITIC derivative-based counterparts. Furthermore, Y6-based OSCs show crucial benefits of low energy loss, good device reproducibility, and satisfactory thickness insensitivity, which are fundamental for the commercialization of OSCs. To date, the highest PCE of Y-series acceptor-based single-junction OSCs has reached 18% through combination with novel polymer donors, which increases this research area to a new stage.[44] In order to get a whole picture of the current development in this field, it would be necessary to provide a systematic review of these A–DA′D–A type acceptor-based high-performance solar cells.

In this review, we firstly introduce several basic concepts and key factors that govern the performance of OSCs. Second, we record the A–DA′D–A type acceptors for high-efficiency OSCs reported in recent years and summarize the molecular design strategies from the state-of-the-art examples. In particular, the correlation between the molecular structure, optoelectronic

Muhammad Umair Ali

Muhammad Umair Ali obtained his MS degree in Physics with specialization in Nanotechnology from International Islamic University, Islamabad, Pakistan, in 2015. He is currently a PhD candidate under the supervision of Professor Huai Yang and Professor Hong Meng at Peking University, Beijing, China. His research focuses on the development of high-performance organic and perovskite optoelectronic devices.

Jingsheng Miao

Jingsheng Miao received his PhD degree in materials physics and chemistry from the South China University of Technology working under the supervision of Prof. Hongbin Wu, Guangzhou, China in 2015. Afterwards, he joined the School of Advanced Materials in Peking University Shenzhen Graduate School as a postdoctoral researcher with Prof. Hong Meng from 2015 until 2017. His research interests include organic solar cells and perovskite solar cells.

Hong Meng

Hong Meng received his PhD degree under the supervision of Prof. Fred Wudl from the University of California Los Angeles (UCLA, USA) in 2002. Currently, he is a professor at the School of Advanced Materials, Peking University Shenzhen Graduate School. He has contributed over 100 peer-reviewed papers in the fields of chemistry and materials science, filed over 50 US patents and 66 Chinese patents, published several book chapters, and co-edited a book titled Organic Light Emitting Materials and Devices. His research fields include organic functional materials synthesis, characterization and devices.

properties, and photovoltaic performance will be addressed. Then, we discuss highly efficient ternary OSCs based on A–DA′D–A type acceptors. Finally, we forecast several orientations for the further development of OSCs toward commercialization.

2. Main factors in determining the performance for OSCs

It is well-recognized that the working mechanism of BHJ OSCs can be divided into five steps: (1) photon absorption and exciton generation, (2) exciton diffusion to the donor/acceptor interface, (3) exciton dissociation into free charge carriers, (4) charge transport to the electrode and (5) charge collection at the electrode.[5,45] To efficiently achieve these steps and enhance the PCE, three important factors need to be considered in terms of light absorption, energy level, and morphology when designing materials and fabricating devices. Generally, light absorption affects step (1) while energy level and morphology are closely related to step (3) and steps (2), (4) and (5), respectively.

2.1 Light absorption

During the aforesaid photophysical processes, the light harvesting process plays a crucially important role in determining the photocurrent. Normally, a donor and an acceptor are mixed together into a blend to form the active layer, where the donor with a medium bandgap mainly covers the absorption region of 450–650 nm while the narrow bandgap acceptor is responsible for the range of 600–1000 nm, therefore fulfilling the light absorption complementarity. As shown in Fig. 2, such combination in non-fullerene solar cells can maximally utilize the solar irradiation, exceeding their fullerene-based counterparts. In this context, several effective methods have been reported to further extend the absorption profile of the active layer, such as thickness-increase of the active layer,[46,47] design of novel acceptor materials with strong NIR absorption and high extinction coefficient,[48–50] introducing a third component to fabricate ternary solar cells[37,38] (detained discussion is provided in Section 3), and adding light-trapping structures in the device.[51,52] It is worth noting that simply taking the "absorption-photocurrent positive correlation law" does not always ensure the aspired device efficiency.[53] In particular, short-circuit current density (J_{SC}) of the device not only depends on the light-harvesting ability of the active layer, but can also be affected by the exciton dissociation, charge transport, and extraction process determined by the micro-morphology. Meanwhile, the enhancement of J_{SC} should not sacrifice the open-circuit voltage (V_{OC}) and fill factor (FF) in a high-performance device.

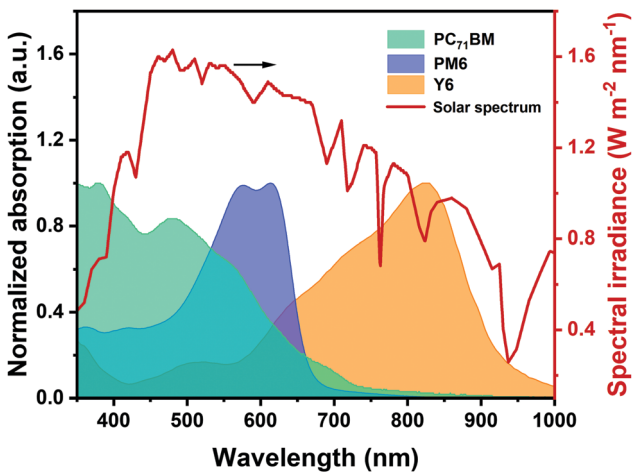

Fig. 2 Solar spectrum (AM 1.5G) and absorption spectra of photovoltaic materials ($PC_{71}BM$, PM6, and Y6) with different bandgaps.

2.2 Energy levels and energy loss

In a typical binary fullerene-based OSC, the highest occupied molecular orbital (HOMO) and lowest unoccupied molecular orbital (LUMO) energy levels of the donor (D) and acceptor (A) should align as depicted in Fig. 3a, in which the energy level offsets between D and A (*i.e.* ΔHOMO and ΔLUMO) need to be larger than 0.3 eV to provide enough driving force to dissociate the exciton. However, recent studies have demonstrated that this limitation can be overcome in NFA-based systems where the energy level offsets can be decreased to approximately 0 eV.[54–56]

Practically, the V_{OC} value of OSCs is proportional to the difference between the LUMO energy level of A and HOMO energy level of D (*i.e.* $|LUMO_A|-|HOMO_D|$). Hence, the trade-off between J_{SC} and V_{OC} should be considered, especially in the pursuit of acceptors with strong NIR absorption. Narrow-bandgap acceptors might bring an improvement of J_{SC}, but would cause reduced V_{OC} values when maintaining the same donor due to the deeper LUMO energy level for the acceptor.

To better understand the origin of voltage loss and increase the value of V_{OC} in different photovoltaic devices, energy loss (E_{loss}) is proposed and defined as follows according to the Shockley–Queisser (SQ) theory:[57,58]

$$\begin{aligned} E_{loss} &= qV_{loss} = E_g - qV_{OC} \\ &= \left(E_g - qV_{OC}^{SQ}\right) + \left(qV_{OC}^{SQ} - qV_{OC}^{rad}\right) + \left(qV_{OC}^{rad} - qV_{OC}\right) \\ &= q\Delta V_{OC}^{SQ} + q\Delta V_{OC}^{rad} + q\Delta V_{OC}^{non\text{-}rad} \\ &= \Delta E_1 + \Delta E_2 + \Delta E_3 \end{aligned} \quad (1)$$

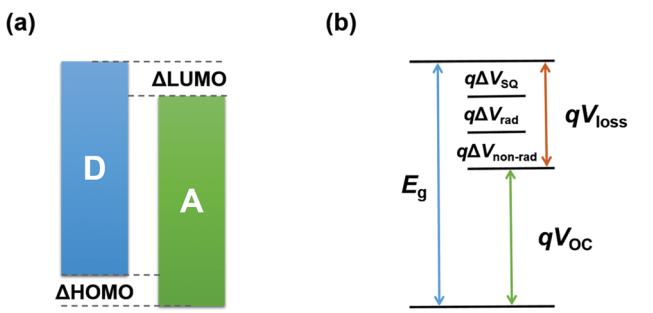

Fig. 3 Schematic illustration of (a) energy levels of the donor and acceptor and (b) various components of energy loss.

Here, E_g is the bandgap of the blend film, q refers to element charge, and V_{OC}^{SQ} is the maximum voltage according to the SQ limit, which can be calculated by the following formula:

$$V_{OC}^{SQ} = \frac{KT}{q}\ln\left(\frac{J_{SC,SQ}}{J_{0,SQ}}+1\right) = \frac{KT}{q}\ln\left(\frac{\int_{E_g}^{\infty}EQE_{PV}(E)\phi_{AM1.5}(E)dE}{\int_{E_g}^{\infty}EQE_{PV}(E)\phi_{BB}(E)dE}+1\right) \quad (2)$$

Here, EQE_{PV} is the external quantum efficiency of the solar cell, and ϕ_{BB} is the blackbody emission flux density. For an ideal solar cell in SQ theory, the EQE_{PV} is a step function which is defined as $EQE_{PV}(E) = 1$ when $E > E_g$, $EQE_{PV}(E) = 0$ when $E < E_g$. Thus, the final formula of the V_{OC}^{SQ} is:

$$V_{OC}^{SQ} = \frac{KT}{q}\ln\left(\frac{\int_{E_g}^{\infty}\phi_{AM1.5}(E)dE}{\int_{E_g}^{\infty}\phi_{BB}(E)dE}+1\right) \quad (3)$$

V_{OC}^{rad} is the voltage when only radiative recombination exists. For practical solar cell materials, the absorption spectrum of the materials is not step function-like, thus, V_{OC}^{rad} is reduced compared with V_{OC}^{SQ}. V_{OC}^{rad} can be calculated using the following formula:

$$V_{OC}^{rad} = \frac{KT}{q}\ln\left(\frac{J_{SC,rad}}{J_{0,rad}}+1\right) = \frac{KT}{q}\ln\left(\frac{\int_{E_g}^{\infty}EQE_{PV}(E)\phi_{AM1.5}(E)dE}{\int_{E_g}^{\infty}EQE_{PV}(E)\phi_{BB}(E)dE}+1\right) \quad (4)$$

In detail, E_{loss} can be categorized into three parts (Fig. 3b): (1) the first term ($\Delta E_1 = E_g - qV_{OC}^{SQ} = q\Delta V_{OC}^{SQ}$, usually 0.25 eV or above) is originated from the radiative recombination because of the absorption above the optical bandgap. This part of the energy loss is unavoidable and can be calculated once the bandgap of the blend is determined; (2) the second part ($\Delta E_2 = qV_{OC}^{SQ} - qV_{OC}^{rad} = q\Delta V_{OC}^{rad}$, in the range of 0.07–0.67 eV) is caused by the additional radiative recombination stemming from the absorption below the bandgap. Compared to silicone and perovskite solar cells, the larger ΔE_2 in OSCs mainly results from the charge transfer (CT) state absorption for the existence of ΔHOMO and ΔLUMO (ΔE_{offset}); and (3) the third loss ($\Delta E_3 = qV_{OC}^{rad} - \Delta V_{OC} = q\Delta V_{OC}^{non\text{-}rad}$, typically 0.26–0.48 eV) is a result of non-radiative recombination; the non-radiative recombination can be originated from the vibronic coupling, traps, and impurities in the actual solar cells.[18] $\Delta V_{OC}^{non\text{-}rad}$ can be calculated using the following formula:

$$q\Delta V_{OC}^{non\text{-}rad} = -kT\ln(EQE_{EL}) \quad (5)$$

EQE_{EL} is the light-emitting diode quantum efficiency of a photovoltaic device when charge carriers are injected into the OSCs in the dark. Clearly, ΔE_3 can be minimized when the luminescence property of the device is improved, which can be summarized as "a great solar cell also needs to be a great light-emitting diode" according to a previous study.[59] Therefore, decreasing the ΔE_{offset} and enhancing the EQE_{EL} are two effective methods to reduce the energy loss (lower than 0.6 eV) and hence, increase the V_{OC} of the device.

2.3 Morphology

Since Heeger *et al.* proposed the BHJ structure of the active layer in 1995,[60] and morphology control came out as a challenging yet intriguing research area for the OSC community. Over time, various techniques and methods, including molecular design,[61–63] composition adjustment of the blend,[64,65] processing solvents and additives,[15,66,67] and post-treatment of the film[14,16,68] have been applied to optimize the micro-morphology of the blend. A favourable BHJ morphology can be described as a scenery that two components (donor and acceptor) form a bi-continuous percolating network with high purity and suitable phase separation with a scale of the exciton free diffusion distance (~20 nm) and hence, promoting the exciton dissociation and reducing the charge recombination. Overall, domain size and continuity, domain purity, and molecular stacking orientation are three key aspects to analyse the morphology in most cases.

Generally, the domain size and continuity in the surface can be visually depicted *via* atomic force microscopy (AFM) and transmission electron microscopy (TEM), as displayed in Fig. 4a and b. Recently, Flory–Huggins interaction parameter (χ) developed from polymer physics was used to predict the miscibility of different components (*e.g.* donor and acceptor) and compare the phase separation of various blend films.[69] A high χ usually stands for stronger phase separation and higher domain purity, which is beneficial for charge generation and transport. In addition, the domain purity can be also characterized with resonant soft X-ray scattering (R-SoXS).

For π-conjugated materials, the highly π electron delocalized molecular surface would give rise to inter-molecular π–π stacking to construct the charge-transporting channels, whose direction is largely related to the molecular orientation. Fig. 4c and d depict two representative molecular packing modes in the device.[70] In the face-on orientation mode, the planar molecules

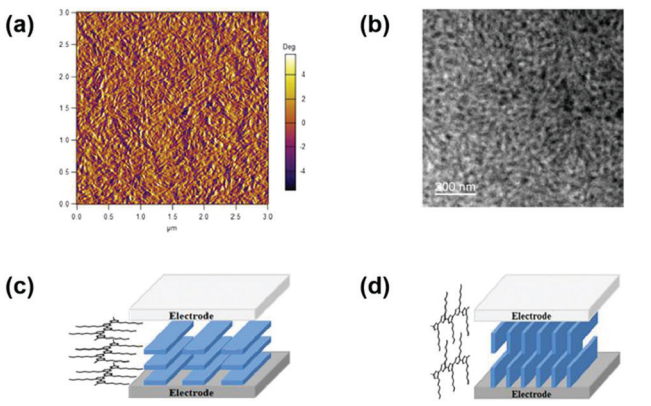

Fig. 4 (a) AFM phase image and (b) TEM image of a typical BHJ blend film. Reproduced with permission.[73] Copyright 2020, American Chemical Society. Schematic illustrations of (c) face-on and (d) edge-on packing mode of active layer materials. Reproduced with permission.[70] Copyright 2016, American Chemical Society.

are aligned stack by stack in parallel with the two electrodes and form straight-forward charge-transporting channels between the electrodes, which is desired for OSCs with a vertical device structure. In contrast, the edge-on orientation would create barriers to vertical charge transport for OSCs. In addition, the molecular orientation can be carefully modulated *via* manipulating the molecular structure and post-treatment, which have been verified in a couple of examples.[62,71,72]

3. Molecular design of A–DA′D–A type acceptors for OSCs

3.1 Molecular structures and packings

As illustrated in Fig. 1, compared with typical A–D–A type NFA (*e.g.* ITIC), Y6 shows quite different molecular configurations, including: (1) Y6 also possesses a highly conjugated backbone but embedded with an electron-deficient moiety in the central fused core. The alternating A–DA′D–A push–pull structure can further facilitate the intra-molecular charge transfer and hence, reduce the bandgap; (2) in Y6, a sp^2-hybridized nitrogen atom is used to replace the sp^3-hybridized carbon in the fused ring, where the lone pair electrons on the perpendicular p orbital can effectively delocalize along the aromatic pyrrole ring. In addition, there is only one side chain attached on each nitrogen atom in Y6, which can reduce the steric hindrance, relative to ITIC; and (3) due to (1) and (2), the whole molecular backbone displays a banana-like shape with mirror symmetry property, thereby affecting its packing behaviour and charge transport property.

The special molecular structure of A–DA′D–A type NFAs leads to their unique molecular packing mode. For example, Liu *et al.* analysed the single crystal of Y6 and found that there are two types of π–π stacking between adjacent molecules, including the end group interactions and the central fused core interactions (as shown in Fig. 5).[74] In particular, the banana-shaped molecules form a zigzag polymer-like conjugated backbone with end group stacking as the major driving force. Similar experimental results were also obtained by He's group. They synthesized a Y-series NFA named BTIC-CF3-γ (as shown in Fig. 6) and revealed that the cooperated π–π interactions from H aggregations of central fused cores and J aggregations of end groups present in its single-crystal can lead to a three-dimensional interpenetrating network, which provides more electron-hopping junctions between adjacent molecules.[75] Consequently, more ordered aggregation and higher charge mobility can be achieved in A–DA′D–A type acceptor based devices compared to their A–D–A structured acceptor counterparts.

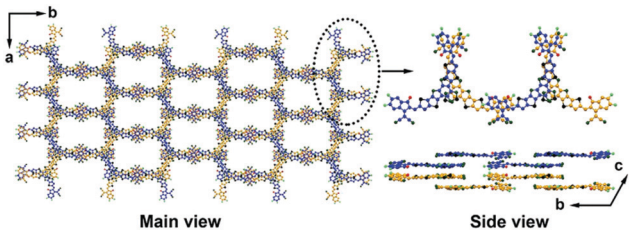

Fig. 5 Molecular packing sketch map of Y6 according to single crystal data (the alkyl chains were omitted for clarity). Reproduced with permission.[74] Copyright 2020, Wiley-VCH.

Typically, A–D–A type acceptors can be reasonably designed and regulated through fused core variation,[69,76–86] side chain engineering,[87–90] and end group modification.[11,73,91–98] As such, similar strategies can be also applied to design novel A–DA′D–A type acceptors, especially the big Y family. In the following text, we will elaborate on these molecular design strategies with selected examples. The chemical structures of donors and acceptors mentioned in the following are shown in Fig. 6 and Fig. S1 (ESI‡) and the detailed optoelectronic and photovoltaic parameters are summarized in Table 1.

3.2 Fused core variation

2,1,3-Benzothiadiazole (BT) and benzotriazole (BTA) are widely utilized electron-deficient building blocks to construct conjugated materials for organic light-emitting diodes,[122,123] organic field-effect transistors,[124] and organic electrochromic devices.[125,126] For OSCs, they are mainly designed as D–A copolymers for donor materials, especially the J-series donors developed by Li *et al.*[127–131] McCulloch and co-workers proposed several BT and BTA based small-molecule acceptors including IDTBR[132] and FBR[133] at an early stage. Nevertheless, the device performance based on these small-molecule acceptors still lags behind for a long period. In 2017, Zou's group introduced a BTA unit into the central core of an A–D–A structural architecture for the first time and obtained a narrow-bandgap n-type acceptor named BZIC, which is the prototype of Y-series acceptors.[99] However, the preliminary results delivered an unsatisfactory PCE of 6.30%, far below that of A–D–A acceptors with indacenodithiophene (IDT) and indacenodithieno[3,2-*b*]-thiophene (IDTT) as the fused core (over 11%) at the same time. Noteworthily, in early 2018, Liu *et al.* proposed the concept of A–D–A′–D–A type non-fullerene electron acceptors with an unfused D–A′–D central core for the first time.[134] The obtained NFA IID-IC (see Fig. S1, ESI‡) with simple synthesis, shows a broad absorption spectrum with the full width at half maximum (FWHM) of 190 nm, much larger than the typical A–D–A structured acceptor ITIC (95 nm). Though the device efficiency based on IID-IC was limited (2.82%) at that time, it motivated another class of NFAs with an unfused A–D–A′–D–A structure for future study.[50]

The breakthrough in the design of A–DA′D–A type NFAs occurred with the discovery of Y6 by further modifying BZIC. In Y6, the electron-deficient BT capped with more extended π-conjugated thieno[3,2-*b*]thiophene (TT) constitutes a DA′D "push–pull" fused core, endowing it with good planarity and narrow bandgap (1.33 eV). Gratifyingly, devices based on PM6:Y6 yielded a record PCE of 15.7% regardless of conventional or inverted device architecture. More importantly, this system can maintain a decent PCE of 13.6% even after increasing the active layer thickness to 300 nm, benefiting from its high electron mobility (see Table 1). Afterwards, Zou *et al.* developed two

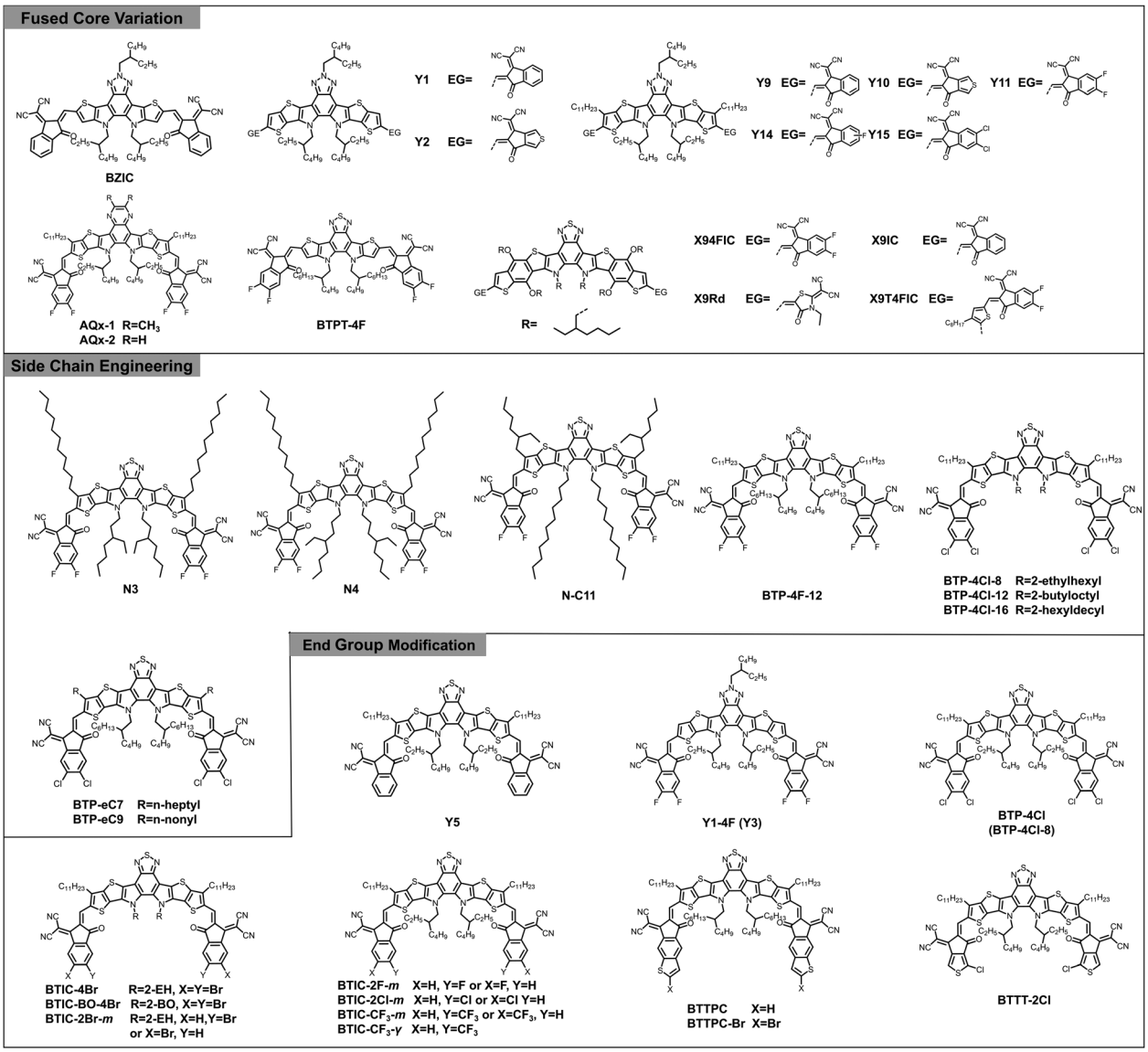

Fig. 6 Chemical structures of A–DA′D–A type acceptors.

other acceptors (Y1 and Y2) by replacing the BT unit with alkyl substituted BTA while retaining the TT unit in Y6.[100] The weaker electron-deficient nature and higher fluorescence properties of the BTA core result in wider bandgap but higher photoluminescence quantum yield (PLQY) of these two materials in comparison with Y6. As expected, low energy losses of 0.57 eV and decent PCEs over 13% were achieved in both devices comprising these acceptors with a polymer donor, PBDB-T. Thus, the successful attempt of DA′D structure sheds light on BT and BTA blocks in designing acceptor materials, which initiated the development of A–DA′D–A type NFAs.

In order to decrease the molecular conformation torsion and further promote the photovoltaic performance of BTA-based molecules, additional alkyl chains are incorporated into the flank of the DA′D fused core along with various end-groups, resulting in a group of superb-performance acceptor materials (Y9,[101] Y10,[102] Y11,[103] Y14,[104] and Y15,[105] see Fig. 6). Take Y11 for example, the fluorinated 1,1-dicyanomethylene-3-indanone (2FIC) with stronger electron-withdrawing properties endows it with smaller optical bandgaps (1.31 eV) and deeper energy levels (−5.69/−3.87 eV) compared with Y1 and Y2. Notably, the highly emissive central core and torsion-free molecular conformation of Y11 are beneficial for mitigating the radiative and non-radiative recombination loss. When blended with PM6 under different processing conditions, the resulting devices exhibit a quite low energy loss of just 0.43–0.51 eV (ΔE_2 = 0.03–0.04 eV, ΔE_3 = 0.17–0.20 eV) and a champion PCE of 16.54%, which is the record efficiency for BTA-based A–DA′D–A structured NFAs.

Following the rational design strategy of Y6, further modifications on the DA′D fused core can be performed from two aspects: one is to search other electron-deficient blocks (A′) to expand this series of acceptors with intriguing properties. For instance, two novel acceptors, AQx-1 and AQx-2 with a

Table 1 Optoelectronic properties and photovoltaic parameters of A–DA′D–A type acceptor-based OSCs

Acceptor	HOMO/LUMO [eV]	E_g^{opt} [eV]	Mobility [10^{-4} cm^2 V^{-1} s^{-1}]	Donor	V_{OC} [V]	J_{SC} [mA cm^2]	FF [%]	PCE [%]	Ref.
Y6	−5.65/−4.10	1.33	2.35[a]	PM6	0.83	25.3	74.8	15.7[c]	43
					0.82	25.2	76.1	15.7[d]	
BZIC	−5.42/−3.88	1.45	1.11[b]	HFQ_x-T	0.84	12.67	59	6.3	99
Y1	−5.45/−3.95	1.44	3.04[b]	PBDB-T	0.87	22.44	69.1	13.42	100
Y2	−5.43/−4.04	1.40	2.08[b]	PBDB-T	0.82	23.56	69.4	13.40	100
Y9	−5.59/−3.78	1.36	6.70[a]	PBDB-T	0.90	23.28	63	13.26	101
Y10	−5.56/−3.76	1.35	4.18[b]	J11	0.89	21.21	71.55	13.46	102
Y11	−5.69/−3.87	1.31	—	PM6	0.833	26.74	74.33	16.54	103
Y14	−5.56/−4.01	1.30	1.00[b]	PBDB-T	0.798	26.15	71.48	14.92	104
Y15	−5.56/−3.96	1.30	5.22[b]	PM6	0.867	23.79	68.49	14.13	105
AQx-1	−5.59/−3.85	1.35	3.72[b]	PM6	0.89	22.18	67.14	13.31	106
AQx-2	−5.62/−3.88	1.35	2.89[b]	PM6	0.86	25.38	76.25	16.64	106
BTPT-4F	−5.73/−4.00	1.45	—	P2F-EHp	0.78	3.20	43.78	1.09	107
X94FIC	−5.58/−4.17	1.25	6.10[b]	PBDB-T	0.73	14.67	66.1	7.08	108
X9IC	−5.53/−4.06	1.29	6.18[b]	PBDB-T	0.86	11.40	63.9	6.29	108
X9Rd	−5.51/−3.80	1.45	6.58[b]	PBDB-T	1.08	6.70	34.1	2.48	108
X9T4FIC	−5.51/−4.10	1.29	5.16[b]	PBDB-T	0.85	7.01	54.1	3.22	108
N3	—	—	4.8[b]	PM6	0.837	25.81	73.9	15.98	109
N4	—	—	1.4[b]	PM6	0.819	25.01	69.9	14.31	109
NC-11	—	—	1.1[b]	PM6	0.852	21.47	70.6	12.91	109
BTP-4F-12	−5.68/−4.06	1.33	7.4[a]	PM6	0.855	25.3	76	16.4	110
BTP-4Cl-8	−5.67/−4.11	1.406	0.286[b]	PM6	0.872	25.2	74.3	16.3	111
BTP-4Cl-12	−5.66/−4.09	1.391	0.292[b]	PM6	0.858	25.6	77.6	17.0	111
BTP-4Cl-16	−5.68/−4.09	1.399	0.310[b]	PM6	0.862	24.2	74.8	15.6	111
BTP-eC7	−5.62/−4.03	1.40	1.28[a]	PM6	0.843	24.1	73.5	14.9	112
BTP-eC9	−5.64/−4.05	1.40	2.70[a]	PM6	0.839	26.2	81.1	17.8	112
Y5	−5.55/−3.87	1.38	2.11[a]	PBDB-T	0.88	22.8	70.2	14.1	113
Y1-4F(Y3)	−5.56/−4.11	1.31	3.01[b]	PM6	0.838	24.80	71.21	14.8	114
BTP-4Cl (BTP-4Cl-8)	−5.68/−4.12	1.400	1.58[b]	PM6	0.867	25.4	75.0	16.5	115
BTIC-4Br	−5.57/−4.11	—	0.23[a], 0.11[b]	PM6	0.85	20.67	69.58	12.20	116
BTIC-BO-4Br	−5.53/−4.09	—	0.81[a], 0.45[b]	PM6	0.86	24.06	67.84	14.03	116
BTIC-2Br-*m*	−5.56/−4.07	—	2.9,[a] 1.1[b]	PM6	0.88	25.03	73.13	16.11	116
BTIC-F-*m*	−5.42/−3.90	1.36	6.7[b]	PM6	0.92	21.41	69.09	13.61	75
BTIC-Cl-*m*	−5.42/−3.91	1.34	3.8[b]	PM6	0.88	21.35	69.70	13.16	75
BTIC-CF_3-*m*	−5.45/−3.97	1.31	0.66[b]	PM6	0.85	24.89	72.32	15.30	75
BTIC-CF_3-γ	−5.45/−3.96	1.30	4.5[b]	PM6	0.85	25.19	72.82	15.59	75
BTTPC	−5.47/−3.78	1.39	5.34[b]	PBDB-T	0.89	22.25	73	14.51	117
BTTPC-Br	−5.54/−3.88	1.37	6.58[b]	PBDB-T	0.86	24.71	71	15.22	117
BTTT-2Cl	−5.61/−3.98	1.36	20.7[b]	PM6	0.904	24.58	67.90	15.10	118
Y16	−5.25/−3.66	—	5.02[b]	PBDB-T	0.914	21.33	66.69	13.00	119
BTP-M	−5.48/−3.81	1.42	5.2[b]	PM6	0.975	8.43	51.80	4.26	120
BP-4F	−5.68/−3.88	—	0.325[b]	PM7	0.880	21.73	76.46	14.62	121

[a] Pristine film: the electron mobility was measured by a space charge limited current (SCLC) method. [b] Blend film: the electron mobility was estimated by an SCLC method. [c] Measured from the conventional device. [d] Measured from the inverted device.

quinoxaline-containing fused core were reported by Zhu *et al.*[106] In comparison with Y6, both of them possess broader bandgaps and up-shifted energy levels, which is derived from the relatively moderate electron-deficient quinoxaline block. In particular, AQ*x*-2 presents strong intermolecular packing and good charge transport properties owing to the quinoidal effect as well as the reduced phase separation morphology of the blend, leading to an outstanding efficiency of 16.64%.

On the other hand, considering the complicated synthesis of alkyl substituted TT (D), developing alternative units with low cost and comparable properties turns out to be an impending task. In one study, Huang *et al.* synthesized a relatively simple A–DA′D–A type acceptor BTPT-4F based on BT and thiophene units.[107] Unfortunately, the efficiency of the P2F-EHp:BTPT-4F device is rather low compared with the Y6-based blend (1.06% *versus* 16.02%), which can be ascribed to the inferior molecular packing property (mainly edge-on-orientated packing) of the BTPT-4F-based blend film according to the grazing-incidence wide-angle X-ray scattering (GIWAXS) results. In another case, Ge *et al.* introduced benzodithophene (BDT) into the A–DA′D–A molecular template and synthesized four new acceptors with different end-groups.[108] Thanks to the good symmetry, highly delocalized π-conjugation, and excellent planarity of BDT, these molecules exhibit high electron mobility and ultra-narrow bandgap, and among them, X94FIC blended with PBDB-T displays a photo-response to 1000 nm, leading to a high J_{SC} of 14.67 mA cm^{-2} and a champion PCE of 7.08%.

3.3 Side chain engineering

In addition to the central DA′D core, side chains are essential moieties in determining the solubility and crystallinity of NFAs. In comparison with the ITIC-type molecules with four identical

chains in a C2 symmetric manner, Y6 possesses two types of side chains in the molecular structure, including two branched alkyl chains on the sp^2 hybridized nitrogen atoms and two straight alkyl chains on the TT unit. The entirely different alignment and arrangement of the side chains motivated researchers to investigate the side chain effect of this new series of acceptors. For example, Yan *et al.* elaborately designed a class of Y6 derivatives, called N3, N4, and N–C11 with alkyl chains of different size, orientation, and branching position (Fig. 6), to study the effect on molecular aggregation behaviours and electronic properties.[109] Intriguingly, N–C11, which is simply designed by swapping the position of 2-ethylhexyl (2-EH) and *n*-undecyl in Y6, showed decreased solubility and large over-aggregated domains in the blend film, leading to a reduced PCE of 12.91%. In contrast, the other two acceptors, especially N3 achieved a balance of good solubility, proper crystallinity, and pronounced face-on stacking orientation and thus, an enhanced efficiency approaching 16% was obtained in the PM6:N3 based device. Overall, these results demonstrated that the alkyl chains with a branched structure attached on the central pyrrole motif play a crucial role in solution processability and charge transport.

Virtually, Y6 is subjected to relatively poor solubility in most common organic solvents and usually processed by chloroform (CF) with high toxicity, which hinders its application from scalable production. To address this shortcoming, several efforts have been devoted. In a representative study, Ge and co-workers developed an A–DA′D–A type acceptor, BTP-4F-12 by carefully increasing the alkyl chains (attached on the central nitrogen atoms) from 2-EH to 2-butyloctyl (2-BO) with almost the same HOMO/LUMO energy levels (−5.68/−4.06 eV) and optical bandgap (1.33 eV) as Y6, whereas the charge transport property was improved due to the enhanced ordering.[110] Furthermore, the enhanced solubility of this newly developed acceptor rendered high-performance solar cells processed with various eco-compatible solvents (THF, *o*-xylene, and 1,2,4-TMB) that yielded a maximum PCE of 16.1% by using T1 as the donor and THF as the solvent. Later, Hou's group designed and synthesized a series of chlorinated acceptors, namely BTP-4Cl-8, BTP-4Cl-12, and BTP-4Cl-16, with extended alkyl chains from 2-EH, to 2-BO, and to 2-hexyldecyl (2-HD). They found that BTP-4Cl-12 based OSCs realized a champion PCE of 17% when pairing with PM6, owing to its balanced aggregation characteristics and solution processability.[111] It should be pointed out that side-chain engineering has limited impact on the optical bandgap and energy levels of these new acceptors, which have been verified in another similar work.[135] Most recently, the same group developed two other small-molecule acceptors, BTP-eC7 and BTP-eC9 by modifying the straight alkyl chains on the TT unit and boosted the device efficiency to nearly 18%, which is the highest value for single-junction OSCs to date.[112]

3.4 End group modification

Among the pool of strategies for molecular modification, end group adjustment has been identified as one of the most common routes due to its good synthetic accessibility and efficient structure–property tunability. Specifically, for Y6 type acceptors, the end groups serve as electron-withdrawing units to strengthen intra-molecular charge transfer and thus reduce the bandgap, but also regulate the energy levels (especially the LUMO energy level) as well as affect the inter-molecular interactions for charge separation and transport.

Y5, composed of a fused ring core (TPBT) identical to Y6 and two non-halogenated end groups, 1,1-dicyanomethylene-3-indanone (INCN), was reported by Zou *et al.* soon after the demonstration of Y6.[113] Because of the weaker electron-withdrawing ability of INCN, Y5 displayed increased HOMO/LUMO energy levels (−5.55/−3.87 eV) and blue-shifted absorption compared to Y6 and an impressive overall efficiency of 14.1% was achieved when blended with a non-halogenated donor, PBDB-T. After that, the same group synthesized a fluorinated small molecule, Y1-4F (Y3) and selected three other materials, Y1, PBDB-T, and PBDB-TF (PM6) to systematically investigate the fluorination effect on energy level alignment and microstructural morphology for Y-series acceptors.[114] Encouragingly, their study provided a guideline that highly efficient OSCs can be achieved by applying both fluorinated or both non-fluorinated donor/acceptor pairs due to well-matched energy levels and miscibility in their respective systems.

Inspired by the success of IT-4Cl, Hou *et al.* conducted chlorination on Y6 *via* simply manipulating the halogen atoms of the end groups and obtained a new acceptor, BTP-4Cl with downshifted LUMO energy level (*ca.* 100 meV) and redshifted optical absorption (*ca.* 20 nm) in comparison with Y6.[115] By virtue of broader light absorption along with reduced energy loss, BTP-4Cl based devices manifested an improved V_{OC} of 0.867 V and J_{SC} of 25.4 mA cm^{-2} compared to Y6, resulting in an increased PCE of 16.5%. After the modifications of Y-series acceptors *via* fluorination and chlorination, He's group implemented bromination to further promote the halogen-substituted strategy in OSCs.[116] Three new acceptors with brominated terminal units, designated as BTIC-4Br, BTIC-BO-4Br, and BTIC-2Br-*m*, were designed and synthesized, among which BTIC-2Br-*m*-based OSCs exhibited the highest PCE of 16.11% with superior V_{OC}, J_{SC}, and FF, resulting from its up-shifted LUMO, complementary and strong absorption, balanced electron/hole mobility, and optimized morphology as evidenced by a series of characterizations. Subsequently, to obtain ultra-narrow bandgap A–DA′D–A type acceptors with extended NIR absorption for further efficiency enhancement, the same group applied a trifluoromethylation approach and synthesized two $-CF_3$ substituted NFAs with bandgaps of only 1.30 eV yet well-matched energy levels with wide-bandgap donor, PM6.[75] Furthermore, the single-crystal results demonstrated that BTIC-CF_3-γ possesses a three-dimensional interpenetrating network with increased electron-hopping sites, which is beneficial for the charge transport. As a result, PM6: BTIC-CF_3-γ OSCs achieved a dramatic PCE of 15.59% with higher J_{SC} and FF compared to its counterparts, BTIC-F-*m*, BTIC-Cl-*m*, and BTIC-CF_3-*m*.

In addition to the modifications by direct-halogenation on the typical terminal group, INCN, constructing novel terminal groups is an alternative strategy to enrich the A–DA′D–A type

NFAs. For instance, Chen *et al.* developed two new end groups, namely TPC and TPC-Br by extending the conjugation with thiophene and bromine moieties.[117] The obtained molecules, BTTPC and BTTPC-Br exhibited small HOMO offsets (0.09 eV and 0.16 eV) in combination with PBDB-T, which is responsible for faster hole transfer feature than that of Y5. Consequently, OSCs based on BTTPC and BTTPC-Br reached impressive efficiencies of 14.51% and 15.22%, respectively, exceeding the INCN end-capped Y5 based device (13.78%). Meanwhile, Min *et al.* reported a NFA, called BTTT-2Cl based on a thiophene and chlorine embedded terminal group, which showed comparable absorption and energy levels with Y6.[118] When combined with PM6, a decent PCE of 13.80% was demonstrated. After introducing 1.0 wt% PZ1 as the additive, the device performance was further improved to 15.10% because of the enhanced molecular ordering and stacking. Remarkably, the trace amount of PZ1 acting as an anchor at the D/A interface could fix the blend microstructure, contributing to its marvelous device thermal stability (retaining 88% of its original efficiency after heating at 150 °C for 800 h). These achievements confirmed that end-group modification is an effective approach to obtain advanced acceptor materials for high-performance OSCs.

4. High-performance ternary OSCs based on A–DA′D–A type acceptors

Since the breakthrough in non-fullerene OSCs obtained by PM6:Y6, this combination has become an ideal candidate for further investigation including interface optimization,[136,137] photophysical process study,[19,138] and device fabrication technology innovation.[74] Among them, the strategy of ternary organic solar cells (TOSCs) by introducing a third component (either a donor or an acceptor) into the active layer, has been demonstrated to be a convenient and effective approach to further boosting the efficiency of binary devices, which can integrate the advantages of existing photovoltaic materials and avoid the complicated process of new material synthesis.

Fig. 7 illustrates three fundamental mechanisms in TOSCs, including charge transfer (CT), energy transfer (ET), and parallel-linkage (PL). For the CT mechanism, the third component with intermediate energy levels functions as a step of the transport pathway at the host D/A interface, which is beneficial for the charge dissociation and transfer process. This is quite common in the cases of donor:acceptor:fullerene TOSCs with enhanced J_{SC}. Differently, in the ET mechanism dominated cases, the third component does not directly participate in the charge generation process but serves as a sunlight absorber to transfer the energy to the host photovoltaic materials through Förster or Dexter energy transfer. The extra charge carriers dissociated from the additional excitons result in a broadened external quantum efficiency (EQE) spectrum and increased J_{SC}. Unlike CT or ET, the PL mechanism (also known as alloyed model) mainly affects the V_{OC} of the photovoltaic device. In this scenario, the additional component possesses a good miscibility and compatibility with one of the host materials (donor or acceptor) and forms an alloy-like phase with averaged energy levels, leading to a varying V_{OC} value scalable with the blend ratio. This strategy has been applied to increase the V_{OC} by incorporating a rationally designed third component. It is worth mentioning that there may exist two different mechanisms in one TOSC. Besides, adopting small molecule acceptors as the third component of TOSCs has been a common choice in recent years owing to their great diversity, excellent device repeatability, and extensive light harvesting. In the following, we will discuss the reported examples from the aspects of fullerene- and non-fullerene-based TOSCs according to the variety of second acceptor; the relevant photovoltaic parameters and mechanisms are summarized in Table 2.

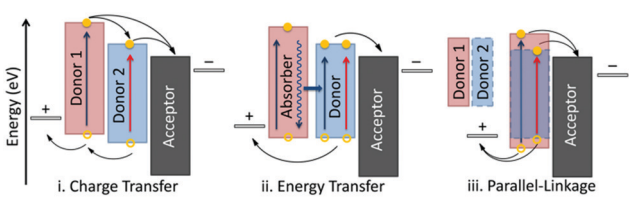

Fig. 7 Three fundamentally different mechanisms of ternary organic solar cells: (i) charge transfer, (ii) energy transfer, and (iii) parallel-linkage. Reproduced with permission.[139] Copyright 2013, American Chemical Society.

As a classic variety of electron acceptors, fullerene derivatives represented by PCBM ([6,6]-phenyl-C60-/C70-butyric acid methyl ester) exhibit strong electron affinity, isotropic charge transport, and high electron mobility in blend films due to their spherical fully conjugated structure. Moreover, they are popular for their good film-forming property, appropriate molecular energy levels, and characteristic absorption in the region of 300–500 nm. These features render PCBM a promising acceptor additive to be utilized in a ternary strategy. In a representative study, Zhan *et al.* systematically investigated the ternary approach with PCBM as the third component in a couple of systems, including PM6:Y6, PM7:Y6, PM6:IT-4F, and PM7:IT-4F; their chemical structures and optoelectronic properties are displayed in Fig. 8a–c.[140] The preliminary results in IT-4F systems indicated that in comparison with $PC_{61}BM$, the introduction of $PC_{71}BM$ obviously enhances the J_{SC} with a simultaneous improvement in FF (see Table 2), which can be ascribed to its broader and stronger light harvesting capability. Then they selected $PC_{71}BM$ as the acceptor additive to fabricate PM6:Y6 and PM7:Y6 based TOSCs and found that V_{OC}, J_{SC}, and FF were all improved at the same time compared to the binary device, yielding decent PCEs of 16.7% and 16.2% in PM6 and PM7 ternary devices, respectively. Further characterization demonstrated that the usage of PCBM helps the host photoactive layer reduce the monomolecular loss, enlarges the sunlight absorption range, and improves the charge transport. These findings are also verified by Ge's group. In particular, they emphasized on the absorption and morphology variation in the PM6:Y6 blend device upon the addition of $PC_{71}BM$.[141] From the UV-vis absorption spectra of the PM6:Y6:$PC_{71}BM$ blend film, it is evident that the maximum absorption peak of Y6 exhibits red shift with an increase in $PC_{71}BM$ ratio,

Table 2 Photovoltaic parameters of ternary OSCs based on A–DA′D–A type acceptors

Binary blend (D:A)	V_{OC} [V]	J_{SC} [mA cm^2]	FF [%]	PCE [%]	Third component	V_{OC} [V]	J_{SC} [mA cm^2]	FF [%]	PCE [%]	Mechanism	Ref.
PM6:IT-4F	0.835	20.6	75.9	13.1	$PC_{61}BM$	0.861	20.8	76.7	13.8	PL	140
PM6:IT-4F	0.835	20.6	75.9	13.1	$PC_{71}BM$	0.859	21.2	76.7	14.0	ET&PL	140
PM7:IT-4F	0.852	20.5	76.8	13.4	$PC_{61}BM$	0.875	20.7	77.2	14.0	PL	140
PM7:IT-4F	0.852	20.5	76.8	13.4	$PC_{71}BM$	0.872	21.2	77.3	14.3	ET&PL	140
PM6:Y6	0.848	24.5	74.6	15.5	$PC_{71}BM$	0.861	25.1	77.2	16.7	ET&PL	140
PM7:Y6	0.875	24.2	72.8	15.4	$PC_{71}BM$	0.884	24.6	74.6	16.2	ET&PL	140
PM6:Y6	0.845	24.89	74.37	15.75	$PC_{71}BM$	0.850	25.70	76.35	16.67	ET&PL	141
PM6:Y6	0.834	24.8	74.1	15.3	$PC_{61}BM$	0.845	25.4	77.0	16.5	PL	142
PM6:N3	0.837	25.81	73.9	15.98	$PC_{71}BM$	0.850	25.71	76.6	16.74	—	109
PM6:Y6	0.844	24.67	74.96	15.61	BTP-M	0.875	26.56	73.46	17.03	PL	120
PM6:Y6	0.84	25.6	74.0	16.0	3TP3T-4F	0.85	26.10	75.4	16.7	ET&PL	143
PM6:Y6	0.84	25.6	74.0	16.0	3TP3T-IC	0.86	25.2	71.6	15.6	—	143
PM6:Y6	0.84	24.78	75.59	15.69	BTIC-CF_3-γ	0.82	26.34	76.62	16.50	—	75
PM6:Y6	0.83	25.10	73	15.2	O-IDTBR	0.85	25.75	76	16.6	CT&PL	144
PM6:Y6	0.857	25.05	71.95	15.45	IDIC	0.868	25.39	74.92	16.51	ET&PL	145
PM7:BP-4F	0.880	21.73	76.46	14.62	MF1	0.891	22.02	78.05	15.31	ET&PL	121
PBDB-T:Y1	0.88	20.4	69.6	12.5	ITCC	0.91	21.4	67.3	13.1	ET	146
PBDB-T:Y16	0.914	21.33	66.69	13.00	MeIC1	0.909	22.76	68.22	14.11	ET&PL	119

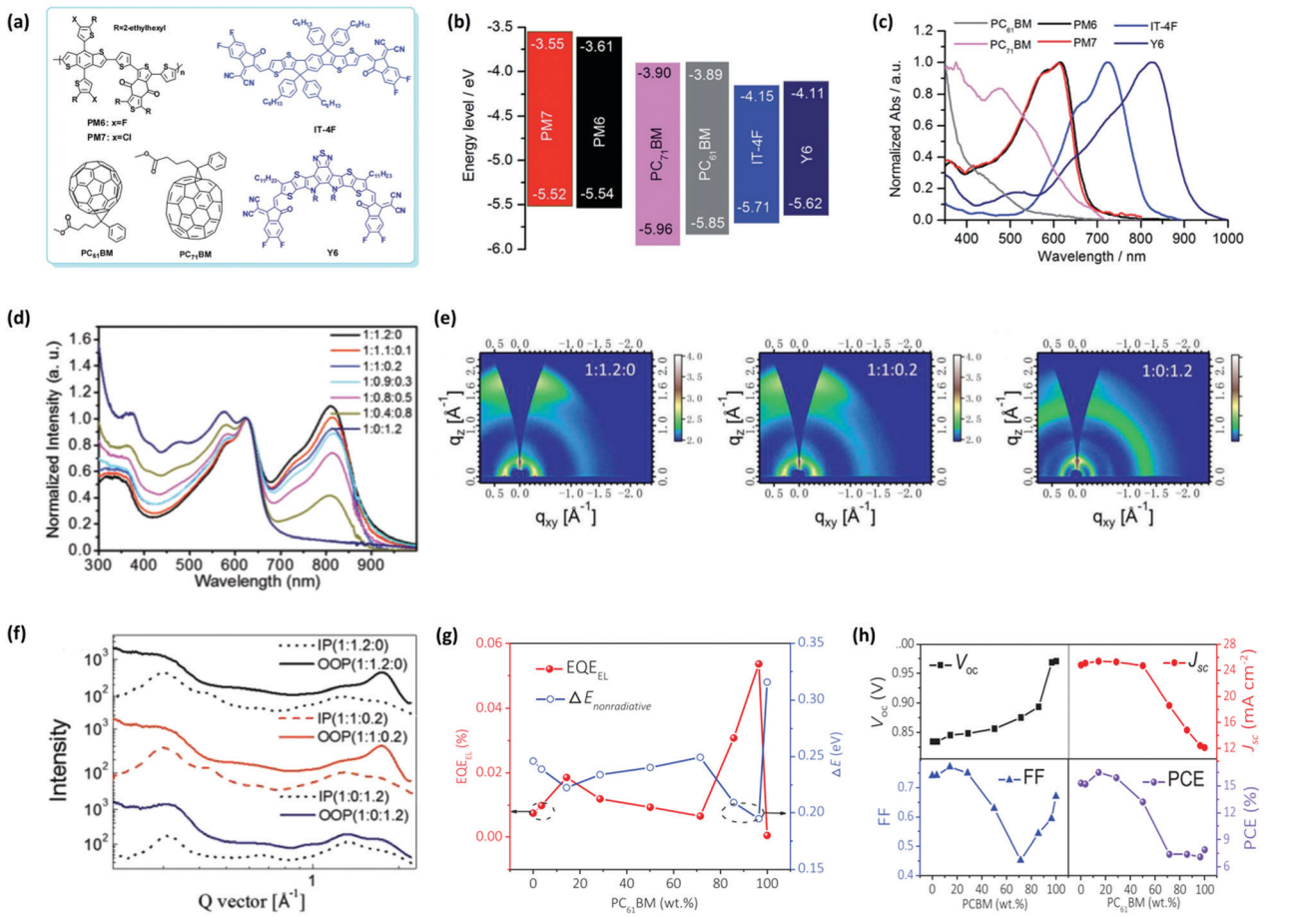

Fig. 8 (a) Chemical structures, (b) energy levels, and (c) normalized UV-vis absorption spectra of the polymer donors, PM6 and PM7, non-fullerene small-molecule acceptors, IT-4F and Y6, and fullerene additives, $PC_{61}BM$ and $PC_{71}BM$. Reproduced with permission.[140] Copyright 2019, The Royal Society of Chemistry. (d) Normalized UV-vis spectra, (e) GIWAXS images, and (f) GIWAXS intensity profiles of PM6:Y6:$PC_{71}BM$ ternary films with different blending ratios. Reproduced with permission.[141] Copyright 2019, Wiley-VCH. (g) EQE_{EL} and non-radiative recombination loss and (h) device parameters, including V_{OC}, J_{SC}, FF, and PCE of PM6:Y6:$PC_{61}BM$ devices containing different $PC_{61}BM$ weight ratios. Reproduced with permission.[142] Copyright 2019, Wiley-VCH.

indicating the energy transfer from $PC_{71}BM$ to Y6. In the meantime, the introduction of $PC_{71}BM$ can improve the coherent length in the out-of-plane (OOP) direction while maintaining the (010) peak of Y6 and (100) peak of PM6 according to the GIWAXS results (Fig. 8e and f). In other words, it increases the intermolecular interactions and thus, induces better charge

transport properties. These changes made by $PC_{71}BM$ concurrently facilitate the enhancement of J_{SC} and FF, thereby increasing the PCE from 15.75% to 16.67%. In another study, Hou *et al.* fabricated PM6:Y6:$PC_{61}BM$ ternary devices and investigated the energy loss effect caused by $PC_{61}BM$.[142] As illustrated in Fig. 8g and h, $PC_{61}BM$ can effectively enhance the EQE_{EL} of the blend film and it reaches a local minimum non-radiative recombination loss at the $PC_{61}BM$ weight ratio of around 20% with synchronous J_{SC} and FF, contributing to an optimum efficiency of 16.5%.

Compared with PCBM, NFAs show stronger light absorption, better miscibility with the host acceptor, and greater device stability when applied in fullerene-free ternary devices. In addition, the tailorable structure with tunable optoelectronic properties of non-fullerene small-molecule acceptors provides a wide range of options for their application in ternary devices involving the above-mentioned mechanisms. Herein, we discuss one representative example for each mechanism to understand their usage in TOSCs.

(1) Guided by the CT model, Baran and co-workers incorporated O-IDTBR (Fig. S1, ESI‡) into the PM6:Y6 binary device as the third component, forming a cascade energy level alignment, as shown in Fig. 9a.[144] The charge carrier mobility of the device (measured by photo-CELIV method) could be enhanced from 8.5×10^{-4} to 1.2×10^{-3} cm^2 V^{-1} s^{-1} upon addition of 15% O-IDTBR. Meanwhile, the trap-assisted recombination loss was reduced after the introduction of O-IDTBR, which was evidenced by V_{OC} *versus* light intensity (P_{in}) characteristics and transient photocurrent (TPC) measurements (Fig. 9b and c). As a result, a remarkable PCE of 16.6% was achieved for the PM6:Y6:3TP3T-4F based TOSCs.

(2) In the case of the ET mechanism dominated example, an A–D–A type small molecule, MF1 (Fig. S1, ESI‡) was employed as the energy transfer agent in the PM7 (PBDB-T-2Cl): BP-4F binary system, whose optical bandgap and absorption spectra lie within the donor and the host acceptor.[121] The overlap between the photoluminescence (PL) spectrum of MF1 and the absorption spectrum of BP-4F (Fig. 9e) also confirmed the efficient energy transfer from MF1 to BP-4F. Besides, the addition of MF1 increased the EQE for the range of 650–750 nm compared to the binary one (Fig. 9f). Consequently, the overall device efficiency was improved to 15.31% from 14.62%, resulting from an enhanced J_{SC}.

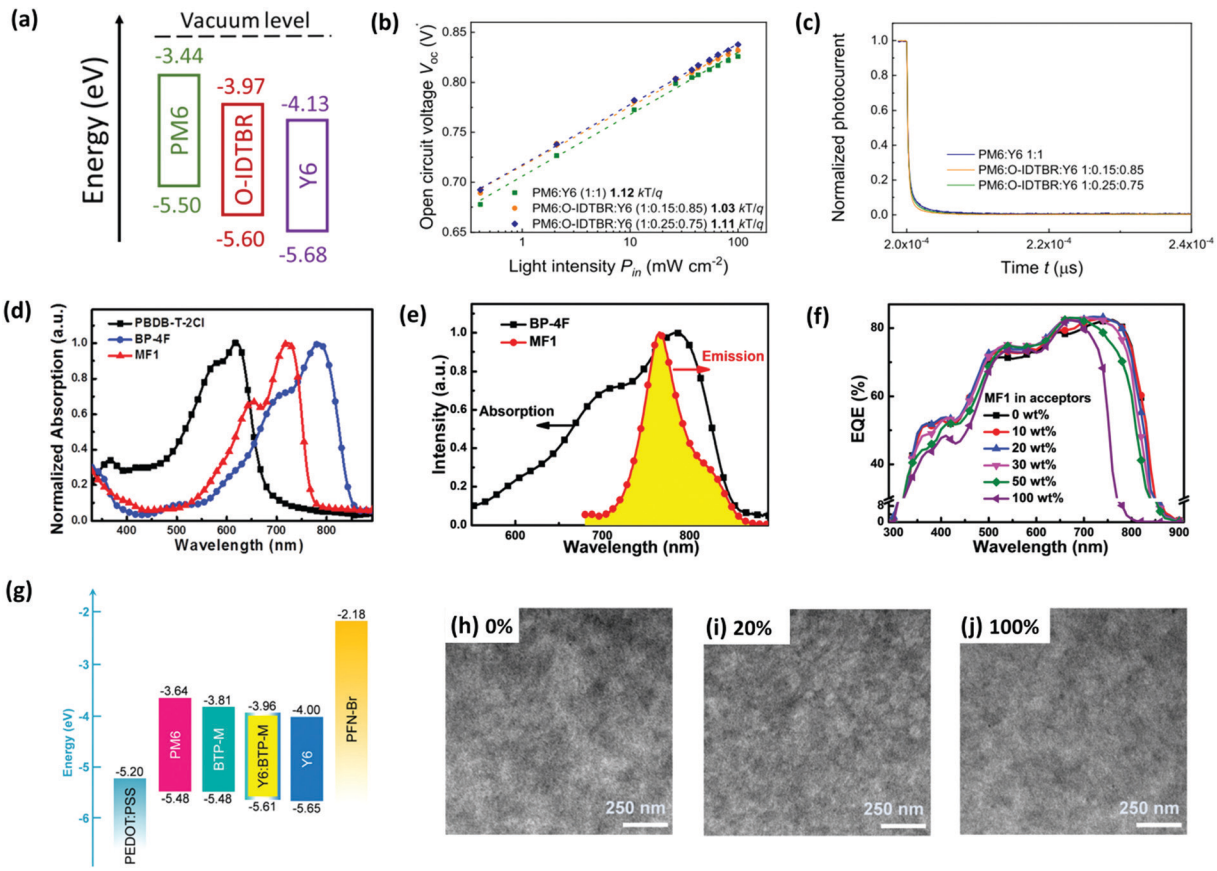

Fig. 9 (a) Energy level diagram of PM6, Y6, and O-IDTBR. (b) V_{OC} *versus* light intensity characteristics and (c) transient photocurrent (TPC) based on optimized binary and ternary OSCs. Reproduced with permission.[143] Copyright 2020, American Chemical Society. (d) Normalized absorption spectra of neat films of PBDB-T-2Cl, MF1, and BP-4F. (e) PL spectrum of neat MF1 film and absorption spectrum of neat BP-4F film. (f) EQE spectra of all OSCs based on PBDB-T-2Cl:MF1:BP-4F with an active layer thickness of about 100 nm. Reproduced with permission.[121] Copyright 2020, The Royal Society of Chemistry. (g) Energy level diagram of the materials used in TOSCs (Y6 : BTP-M = 4 : 1, by wt%). (h–j) TEM images of two binary blends (0% and 100%) and the optimal ternary blend (20%). Reproduced with permission.[120] Copyright 2020, The Royal Society of Chemistry.

(3) Chen *et al.* elaborately designed and synthesized a new A–DA′D–A type acceptor, named BTP-M (see Fig. S1, ESI‡) as the third component for the binary blend consisting of PM6 and Y6.[120] Due to the high structure similarity between BTP-M and Y6, these two materials can mix well with each other and form an alloy-like phase. Moreover, thanks to the higher energy levels of BTP-M, this alloy-like composite shows increased LUMO compared to Y6, which can alleviate the energy loss and thus improve the V_{OC} owing to the decreased LUMO offset between PM6 and the composite. Moreover, the introduction of BTP-M with lower crystallinity and weaker intermolecular interactions can effectively remedy the over-aggregation behaviour of Y6 and optimize the morphological domain size (see Fig. 9g–j), which is responsible for the enhanced J_{SC}. Consequently, a remarkable PCE of 17.03% was obtained for the ternary device, which is one of the best reported PCEs achieved by single-junction fullerene-free OSCs.

Throughout the overview of TOSCs based on A–DA′D–A type acceptors, the ternary strategy can significantly enhance the value of one or more photovoltaic parameters without obviously sacrificing the residual ones and thereby achieves an increased efficiency. Further investigations and more efforts are desired to keep this research field prosperous and thriving.

Conclusions

In the last two years, A–DA′D–A structured NFAs represented by Y6 have emerged as a new and fascinating class of acceptors to realize OSCs with record efficiency. In this article, we offered an overview of Y6 and its derivatives, from the aspects of key factors in determining device performance, molecular design strategies, and efficiency improvement by means of ternary solar cells. Specifically, the enhanced electron push–pull structure and highly emissive fused central core of these novel materials endow the active layer with strong near-infrared light absorption and low energy loss, concurrently leading to high J_{SC}, V_{OC}, and hence, achieving a benchmark PCE of over 16%. Periodical achievements demonstrate that Y-series NFAs have broken up the dominating role of classical A–D–A type ITIC-derivatives in the field of OSCs and came out as promising candidates for future industrialization.

To promote the commercial applications of OSCs, several crucial issues and research areas are desired for further investigation. We spotlight some of the future research directions in the following: (1) synthesis of new NFAs with an A–DA′D–A structure. As the last generation star molecule, ITIC showed a moderate device performance (PCE = 6.80%) in the beginning, whereas it realized a prominent efficiency of over 14% after years of molecular structure optimization. Analogously, Y6 is currently at the nascent stage presently and hence, further developing this new category of NFAs with intriguing properties to improve the efficiency is imperative and anticipated, in consideration of their good structure tunability. (2) To design and synthesize novel donor materials for combination with A–DA′D–A type NFAs. Currently, most of the highly efficient OSCs are achieved by copolymer donors based on BDT and benzo-[1,2-*c*:4,5-*c*′]dithiophene-4,8-dione (BDD), such as PBDB-T, PBDB-T-2F (PM6), and PBDB-T-2Cl (PM7), which have been extensively utilized in the ITIC derivatives system for a long period. Therefore, in addition to the design of new acceptors, developing new donors with deeper HOMO and appropriate crystallinity and miscibility in the blend is another potential method to synergistically promote the performance of OSCs. Inspiringly, several research groups have paid attention to this field and achieved gratifying progress, represented by Pt10,[147] S1,[148] D16,[149] and D18.[44] (3) Fabricating ternary and tandem OSCs based on A–DA′D–A type NFAs to further boost the photovoltaic performance since the record efficiency of binary single-junction OSCs has been up to 18%. (4) Further exploring the potential of large-area manufacturing of OSCs with decent efficiency and high yield. The key is to develop air- and thickness-insensitive and post-treatment-free photovoltaic layer materials, eco-friendly processing solvents, compatible and flexible substrates, and ink-jet printing techniques. (5) Enhancing the device stability of new-generation NFAs. In view of the extended and conjugated aromatic fused ring features of Y-series molecules, they are susceptible to the photochemical degradation induced by UV-light, heat, moisture, and oxygen in the surroundings. Thus, photochemical stability and fixed morphological micro-structure are preferable characteristics for the active layer blend along with advanced device-packaging techniques, which can meet the requirements of long-term operation in OSC applications.

Conflicts of interest

There are no conflicts to declare.

Acknowledgements

This work was supported by the National Natural Science Foundation of China (51903005), the Key-Area Research and Development Program of Guangdong Province (2019B010924003), China (Shenzhen)-Canada Technology Collaboration Project (GJHZ20180420180725249), Shenzhen Peacock Plan (KQTD-2014062714543296), Shenzhen Hong Kong Innovation Circle joint R & D project (SGLH20161212101631809), and China (Shenzhen)-United States Technology Collaboration Project (GJHZ20180928163206500).

Notes and references

1 G. Zhang, J. Zhao, P. C. Y. Chow, K. Jiang, J. Zhang, Z. Zhu, J. Zhang, F. Huang and H. Yan, Nonfullerene Acceptor Molecules for Bulk Heterojunction Organic Solar Cells, *Chem. Rev.*, 2018, **118**, 3447–3507.
2 C. Yan, S. Barlow, Z. Wang, H. Yan, A. K. Y. Jen, S. R. Marder and X. Zhan, Non-fullerene acceptors for organic solar cells, *Nat. Rev. Mater.*, 2018, **3**, 18003.
3 A. Wadsworth, M. Moser, A. Marks, M. S. Little, N. Gasparini, C. J. Brabec, D. Baran and I. McCulloch, Critical review of the

molecular design progress in non-fullerene electron acceptors towards commercially viable organic solar cells, *Chem. Soc. Rev.*, 2019, **48**, 1596–1625.
4 R. Xue, J. Zhang, Y. Li and Y. Li, Organic Solar Cell Materials toward Commercialization, *Small*, 2018, **14**, 1801793.
5 P. Cheng, G. Li, X. Zhan and Y. Yang, Next-generation organic photovoltaics based on non-fullerene acceptors, *Nat. Photonics*, 2018, **12**, 131–142.
6 S. Li, W. Liu, C. Z. Li, M. Shi and H. Chen, Efficient Organic Solar Cells with Non-Fullerene Acceptors, *Small*, 2017, **13**, 1701120.
7 L. Lu, T. Zheng, Q. Wu, A. M. Schneider, D. Zhao and L. Yu, Recent Advances in Bulk Heterojunction Polymer Solar Cells, *Chem. Rev.*, 2015, **115**, 12666–12731.
8 T. Yang, M. Wang, C. Duan, X. Hu, L. Huang, J. Peng, F. Huang and X. Gong, Inverted polymer solar cells with 8.4% efficiency by conjugated polyelectrolyte, *Energy Environ. Sci.*, 2012, **5**, 8208–8214.
9 Z.-G. Zhang, B. Qi, Z. Jin, D. Chi, Z. Qi, Y. Li and J. Wang, Perylene diimides: a thickness-insensitive cathode interlayer for high performance polymer solar cells, *Energy Environ. Sci.*, 2014, **7**, 1966–1973.
10 Y. Zhang, H. Yao, S. Zhang, Y. Qin, J. Zhang, L. Yang, W. Li, Z. Wei, F. Gao and J. Hou, Fluorination vs. chlorination: a case study on high performance organic photovoltaic materials, *Sci. China: Chem.*, 2018, **61**, 1328–1337.
11 W. Zhao, S. Li, H. Yao, S. Zhang, Y. Zhang, B. Yang and J. Hou, Molecular Optimization Enables over 13% Efficiency in Organic Solar Cells, *J. Am. Chem. Soc.*, 2017, **139**, 7148–7151.
12 Y. Lin, J. Wang, Z. G. Zhang, H. Bai, Y. Li, D. Zhu and X. Zhan, An electron acceptor challenging fullerenes for efficient polymer solar cells, *Adv. Mater.*, 2015, **27**, 1170–1174.
13 D. Qian, L. Ye, M. Zhang, Y. Liang, L. Li, Y. Huang, X. Guo, S. Zhang, Z. A. Tan and J. Hou, Design, Application, and Morphology Study of a New Photovoltaic Polymer with Strong Aggregation in Solution State, *Macromolecules*, 2012, **45**, 9611–9617.
14 G. Li, V. Shrotriya, J. Huang, Y. Yao, T. Moriarty, K. Emery and Y. Yang, High-efficiency solution processable polymer photovoltaic cells by self-organization of polymer blends, *Nat. Mater.*, 2005, **4**, 864–868.
15 J. Peet, J. Y. Kim, N. E. Coates, W. L. Ma, D. Moses, A. J. Heeger and G. C. Bazan, Efficiency enhancement in low-bandgap polymer solar cells by processing with alkane dithiols, *Nat. Mater.*, 2007, **6**, 497–500.
16 M. Shin, H. Kim, J. Park, S. Nam, K. Heo, M. Ree, C.-S. Ha and Y. Kim, Abrupt Morphology Change upon Thermal Annealing in Poly(3-Hexylthiophene)/Soluble Fullerene Blend Films for Polymer Solar Cells, *Adv. Funct. Mater.*, 2010, **20**, 748–754.
17 X. Liu, Y. Li, K. Ding and S. Forrest, Energy Loss in Organic Photovoltaics: Nonfullerene Versus Fullerene Acceptors, *Phys. Rev. Appl.*, 2019, **11**, 024060.
18 M. Azzouzi, J. Yan, T. Kirchartz, K. Liu, J. Wang, H. Wu and J. Nelson, Nonradiative Energy Losses in Bulk-Heterojunction Organic Photovoltaics, *Phys. Rev. X*, 2018, **8**, 031055.
19 A. Karki, J. Vollbrecht, A. L. Dixon, N. Schopp, M. Schrock, G. N. M. Reddy and T. Q. Nguyen, Understanding the High Performance of over 15% Efficiency in Single-Junction Bulk Heterojunction Organic Solar Cells, *Adv. Mater.*, 2019, **31**, 1903868.
20 J. Zhao, Y. Li, G. Yang, K. Jiang, H. Lin, H. Ade, W. Ma and H. Yan, Efficient organic solar cells processed from hydrocarbon solvents, *Nat. Energy*, 2016, **1**, 15027.
21 P. Cheng, J. Hou, Y. Li and X. Zhan, Layer-by-Layer Solution-Processed Low-Bandgap Polymer-PC61BM Solar Cells with High Efficiency, *Adv. Energy Mater.*, 2014, **4**, 1301349.
22 Y. He, H.-Y. Chen, J. Hou and Y. Li, Indene−C60 Bisadduct: A New Acceptor for High-Performance Polymer Solar Cells, *J. Am. Chem. Soc.*, 2010, **132**, 1377–1382.
23 B. Kan, H. Feng, H. Yao, M. Chang, X. Wan, C. Li, J. Hou and Y. Chen, A chlorinated low-bandgap small-molecule acceptor for organic solar cells with 14.1% efficiency and low energy loss, *Sci. China: Chem.*, 2018, **61**, 1307–1313.
24 H. Zhang, H. Yao, J. Hou, J. Zhu, J. Zhang, W. Li, R. Yu, B. Gao, S. Zhang and J. Hou, Over 14% Efficiency in Organic Solar Cells Enabled by Chlorinated Nonfullerene Small-Molecule Acceptors, *Adv. Mater.*, 2018, **30**, 1800613.
25 S. Zhang, Y. Qin, J. Zhu and J. Hou, Over 14% Efficiency in Polymer Solar Cells Enabled by a Chlorinated Polymer Donor, *Adv. Mater.*, 2018, **30**, 1800868.
26 Y. Zhang, H. Yao, S. Zhang, Y. Qin, J. Zhang, L. Yang, W. Li, Z. Wei, F. Gao and J. Hou, Fluorination vs. chlorination: a case study on high performance organic photovoltaic materials, *Sci. China: Chem.*, 2018, **61**, 1328–1337.
27 J. Lee, S.-J. Ko, M. Seifrid, H. Lee, C. McDowell, B. R. Luginbuhl, A. Karki, K. Cho, T.-Q. Nguyen and G. C. Bazan, Design of Nonfullerene Acceptors with Near-Infrared Light Absorption Capabilities, *Adv. Energy Mater.*, 2018, **8**, 1801209.
28 H. Yao, Y. Cui, R. Yu, B. Gao, H. Zhang and J. Hou, Design, Synthesis, and Photovoltaic Characterization of a Small Molecular Acceptor with an Ultra-Narrow Band Gap, *Angew. Chem., Int. Ed.*, 2017, **56**, 3045–3049.
29 Y. Cui, C. Yang, H. Yao, J. Zhu, Y. Wang, G. Jia, F. Gao and J. Hou, Efficient Semitransparent Organic Solar Cells with Tunable Color enabled by an Ultralow-Bandgap Nonfullerene Acceptor, *Adv. Mater.*, 2017, **29**, 1703080.
30 S. Dai, T. Li, W. Wang, Y. Xiao, T. K. Lau, Z. Li, K. Liu, X. Lu and X. Zhan, Enhancing the Performance of Polymer Solar Cells via Core Engineering of NIR-Absorbing Electron Acceptors, *Adv. Mater.*, 2018, **30**, 1706571.
31 H. Li, Z. Xiao, L. Ding and J. Wang, Thermostable single-junction organic solar cells with a power conversion efficiency of 14.62%, *Sci. Bull.*, 2018, **63**, 340–342.
32 D. Liu, T. Wang, X. Ke, N. Zheng, Z. Chang, Z. Xie and Y. Liu, Ultra-narrow bandgap non-fullerene acceptors for organic solar cells with low energy loss, *Mater. Chem. Front.*, 2019, **3**, 2157–2163.
33 Z. Yao, X. Liao, K. Gao, F. Lin, X. Xu, X. Shi, L. Zuo, F. Liu, Y. Chen and A. K. Y. Jen, Dithienopicenocarbazole-Based Acceptors for Efficient Organic Solar Cells with

Optoelectronic Response Over 1000 nm and an Extremely Low Energy Loss, *J. Am. Chem. Soc.*, 2018, **140**, 2054–2057.

34 Y. Chen, Y. Qin, Y. Wu, C. Li, H. Yao, N. Liang, X. Wang, W. Li, W. Ma and J. Hou, From Binary to Ternary: Improving the External Quantum Efficiency of Small-Molecule Acceptor-Based Polymer Solar Cells with a Minute Amount of Fullerene Sensitization, *Adv. Energy Mater.*, 2017, **7**, 1700328.

35 Z. Xiao, X. Jia and L. Ding, Ternary organic solar cells offer 14% power conversion efficiency, *Sci. Bull.*, 2017, **62**, 1562–1564.

36 J. Mai, Y. Xiao, G. Zhou, J. Wang, J. Zhu, N. Zhao, X. Zhan and X. Lu, Hidden Structure Ordering Along Backbone of Fused-Ring Electron Acceptors Enhanced by Ternary Bulk Heterojunction, *Adv. Mater.*, 2018, **30**, 1802888.

37 P. Xue, Y. Xiao, T. Li, S. Dai, B. Jia, K. Liu, J. Wang, X. Lu, R. P. S. Han and X. Zhan, High-performance ternary organic solar cells with photoresponses beyond 1000 nm, *J. Mater. Chem. A*, 2018, **6**, 24210–24215.

38 M. Zhang, Z. Xiao, W. Gao, Q. Liu, K. Jin, W. Wang, Y. Mi, Q. An, X. Ma, X. Liu, C. Yang, L. Ding and F. Zhang, Over 13% Efficiency Ternary Nonfullerene Polymer Solar Cells with Tilted Up Absorption Edge by Incorporating a Medium Bandgap Acceptor, *Adv. Energy Mater.*, 2018, **8**, 1801968.

39 Y. Cui, H. Yao, B. Gao, Y. Qin, S. Zhang, B. Yang, C. He, B. Xu and J. Hou, Fine-Tuned Photoactive and Interconnection Layers for Achieving over 13% Efficiency in a Fullerene-Free Tandem Organic Solar Cell, *J. Am. Chem. Soc.*, 2017, **139**, 7302–7309.

40 S. Chen, H. Yao, B. Hu, G. Zhang, L. Arunagiri, L.-K. Ma, J. Huang, J. Zhang, Z. Zhu, F. Bai, W. Ma and H. Yan, A Nonfullerene Semitransparent Tandem Organic Solar Cell with 10.5% Power Conversion Efficiency, *Adv. Energy Mater.*, 2018, **8**, 1800529.

41 L. Meng, Y. Zhang, X. Wan, C. Li, X. Zhang, Y. Wang, X. Ke, Z. Xiao, L. Ding, R. Xia, H. L. Yip, Y. Cao and Y. Chen, Organic and solution-processed tandem solar cells with 17.3% efficiency, *Science*, 2018, **361**, 1094–1098.

42 G. Liu, J. Jia, K. Zhang, X. E. Jia, Q. Yin, W. Zhong, L. Li, F. Huang and Y. Cao, 15% Efficiency Tandem Organic Solar Cell Based on a Novel Highly Efficient Wide-Bandgap Nonfullerene Acceptor with Low Energy Loss, *Adv. Energy Mater.*, 2019, **9**, 1803657.

43 J. Yuan, Y. Zhang, L. Zhou, G. Zhang, H.-L. Yip, T.-K. Lau, X. Lu, C. Zhu, H. Peng, P. A. Johnson, M. Leclerc, Y. Cao, J. Ulanski, Y. Li and Y. Zou, Single-Junction Organic Solar Cell with over 15% Efficiency Using Fused-Ring Acceptor with Electron-Deficient Core, *Joule*, 2019, **3**, 1140–1151.

44 Q. Liu, Y. Jiang, K. Jin, J. Qin, J. Xu, W. Li, J. Xiong, J. Liu, Z. Xiao, K. Sun, S. Yang, X. Zhang and L. Ding, 18% Efficiency organic solar cells, *Sci. Bull.*, 2020, **65**, 272–275.

45 A. J. Heeger, 25th anniversary article: Bulk heterojunction solar cells: understanding the mechanism of operation, *Adv. Mater.*, 2014, **26**, 10–27.

46 Y. Jin, Z. Chen, M. Xiao, J. Peng, B. Fan, L. Ying, G. Zhang, X.-F. Jiang, Q. Yin, Z. Liang, F. Huang and Y. Cao, Thick Film Polymer Solar Cells Based on Naphtho[1,2-*c*:5,6-*c*]-bis[1,2,5]thiadiazole Conjugated Polymers with Efficiency over 11%, *Adv. Energy Mater.*, 2017, **7**, 1700944.

47 C. Sun, F. Pan, H. Bin, J. Zhang, L. Xue, B. Qiu, Z. Wei, Z.-G. Zhang and Y. Li, A low cost and high performance polymer donor material for polymer solar cells, *Nat. Commun.*, 2018, **9**, 743.

48 F.-X. Chen, J.-Q. Xu, Z.-X. Liu, M. Chen, R. Xia, Y. Yang, T.-K. Lau, Y. Zhang, X. Lu, H.-L. Yip, A. K. Y. Jen, H. Chen and C.-Z. Li, Near-Infrared Electron Acceptors with Fluorinated Regioisomeric Backbone for Highly Efficient Polymer Solar Cells, *Adv. Mater.*, 2018, **30**, 1803769.

49 S. Li, L. Zhan, T.-K. Lau, Z.-P. Yu, W. Yang, T. R. Andersen, Z. Fu, C.-Z. Li, X. Lu, M. Shi and H. Chen, Near-Infrared Nonfullerene Acceptors Based on Benzobis(thiazole) Unit for Efficient Organic Solar Cells with Low Energy Loss, *Small Methods*, 2019, **3**, 1900531.

50 S. Pang, X. Zhou, S. Zhang, H. Tang, S. Dhakal, X. Gu, C. Duan, F. Huang and Y. Cao, Nonfused Nonfullerene Acceptors with an A-D-A′-D-A Framework and a Benzothiadiazole Core for High-Performance Organic Solar Cells, *ACS Appl. Mater. Interfaces*, 2020, **12**, 16531–16540.

51 J. Wu, X. Che, H.-C. Hu, H. Xu, B. Li, Y. Liu, J. Li, Y. Ni, X. Zhang and X. Ouyang, Organic solar cells based on cellulose nanopaper from agroforestry residues with an efficiency of over 16% and effectively wide-angle light capturing, *J. Mater. Chem. A*, 2020, **8**, 5442–5448.

52 F.-S. Zu, X.-B. Shi, J. Liang, M.-F. Xu, C.-S. Lee, Z.-K. Wang and L.-S. Liao, Efficient optical absorption enhancement in organic solar cells by using a 2-dimensional periodic light trapping structure, *Appl. Phys. Lett.*, 2014, **104**, 243904.

53 M. Zhang, W. Gao, F. Zhang, Y. Mi, W. Wang, Q. An, J. Wang, X. Ma, J. Miao, Z. Hu, X. Liu, J. Zhang and C. Yang, Efficient ternary non-fullerene polymer solar cells with PCE of 11.92% and FF of 76.5%, *Energy Environ. Sci.*, 2018, **11**, 841–849.

54 J. Liu, S. Chen, D. Qian, B. Gautam, G. Yang, J. Zhao, J. Bergqvist, F. Zhang, W. Ma, H. Ade, O. Inganäs, K. Gundogdu, F. Gao and H. Yan, Fast charge separation in a non-fullerene organic solar cell with a small driving force, *Nat. Energy*, 2016, **1**, 16089.

55 S. Li, L. Zhan, C. Sun, H. Zhu, G. Zhou, W. Yang, M. Shi, C. Z. Li, J. Hou, Y. Li and H. Chen, Highly Efficient Fullerene-Free Organic Solar Cells Operate at Near Zero Highest Occupied Molecular Orbital Offsets, *J. Am. Chem. Soc.*, 2019, **141**, 3073–3082.

56 H. Fu, Y. Wang, D. Meng, Z. Ma, Y. Li, F. Gao, Z. Wang and Y. Sun, Suppression of Recombination Energy Losses by Decreasing the Energetic Offsets in Perylene Diimide-Based Nonfullerene Organic Solar Cells, *ACS Energy Lett.*, 2018, **3**, 2729–2735.

57 D. Qian, Z. Zheng, H. Yao, W. Tress, T. R. Hopper, S. Chen, S. Li, J. Liu, S. Chen, J. Zhang, X. K. Liu, B. Gao, L. Ouyang, Y. Jin, G. Pozina, I. A. Buyanova, W. M. Chen, O. Inganas, V. Coropceanu, J. L. Bredas, H. Yan, J. Hou, F. Zhang, A. A. Bakulin and F. Gao, Design rules for minimizing

voltage losses in high-efficiency organic solar cells, *Nat. Mater.*, 2018, **17**, 703–709.

58 J. Benduhn, K. Tvingstedt, F. Piersimoni, S. Ullbrich, Y. Fan, M. Tropiano, K. A. McGarry, O. Zeika, M. K. Riede, C. J. Douglas, S. Barlow, S. R. Marder, D. Neher, D. Spoltore and K. Vandewal, Intrinsic non-radiative voltage losses in fullerene-based organic solar cells, *Nat. Energy*, 2017, **2**, 17053.

59 J. Hou, O. Inganas, R. H. Friend and F. Gao, Organic solar cells based on non-fullerene acceptors, *Nat. Mater.*, 2018, **17**, 119–128.

60 G. Yu, J. Gao, J. C. Hummelen, F. Wudl and A. J. Heeger, Polymer Photovoltaic Cells: Enhanced Efficiencies via a Network of Internal Donor-Acceptor Heterojunctions, *Science*, 1995, **270**, 1789–1791.

61 Y. Kim, S. Cook, S. M. Tuladhar, S. A. Choulis, J. Nelson, J. R. Durrant, D. D. C. Bradley, M. Giles, I. McCulloch, C.-S. Ha and M. Ree, A strong regioregularity effect in self-organizing conjugated polymer films and high-efficiency polythiophene:fullerene solar cells, *Nat. Mater.*, 2006, **5**, 197–203.

62 W. Li, S. Albrecht, L. Yang, S. Roland, J. R. Tumbleston, T. McAfee, L. Yan, M. A. Kelly, H. Ade, D. Neher and W. You, Mobility-controlled performance of thick solar cells based on fluorinated copolymers, *J. Am. Chem. Soc.*, 2014, **136**, 15566–15576.

63 I. Osaka, M. Saito, T. Koganezawa and K. Takimiya, Thiophene-thiazolothiazole copolymers: significant impact of side chain composition on backbone orientation and solar cell performances, *Adv. Mater.*, 2014, **26**, 331–338.

64 S. H. Park, A. Roy, S. Beaupré, S. Cho, N. Coates, J. S. Moon, D. Moses, M. Leclerc, K. Lee and A. J. Heeger, Bulk heterojunction solar cells with internal quantum efficiency approaching 100%, *Nat. Photonics*, 2009, **3**, 297–302.

65 P. Cheng, Y. Li and X. Zhan, Efficient ternary blend polymer solar cells with indene-C60 bisadduct as an electron-cascade acceptor, *Energy Environ. Sci.*, 2014, **7**, 2005–2011.

66 A. Li, X. Miao and X. Deng, Strong electron acceptor additive for achieving efficient polymer solar cells with P3HT: PCBM films by a quick drying process, *Synth. Met.*, 2013, **168**, 43–47.

67 K. Schmidt, C. J. Tassone, J. R. Niskala, A. T. Yiu, O. P. Lee, T. M. Weiss, C. Wang, J. M. Frechet, P. M. Beaujuge and M. F. Toney, A mechanistic understanding of processing additive-induced efficiency enhancement in bulk heterojunction organic solar cells, *Adv. Mater.*, 2014, **26**, 300–305.

68 C. J. Ko, Y. K. Lin and F. C. Chen, Microwave Annealing of Polymer Photovoltaic Devices, *Adv. Mater.*, 2007, **19**, 3520–3523.

69 H. Feng, Y. Q. Q. Yi, X. Ke, J. Yan, Y. Zhang, X. Wan, C. Li, N. Zheng, Z. Xie and Y. Chen, New Anthracene-Fused Nonfullerene Acceptors for High-Efficiency Organic Solar Cells: Energy Level Modulations Enabling Match of Donor and Acceptor, *Adv. Energy Mater.*, 2019, **9**, 1803541.

70 C. Guo, Y. Lee, Y.-H. Lin, J. Strzalka, C. Wang, A. Hexemer, C. Jaye, D. A. Fischer, R. Verduzco, Q. Wang and E. D. Gomez, Photovoltaic Performance of Block Copolymer Devices Is Independent of the Crystalline Texture in the Active Layer, *Macromolecules*, 2016, **49**, 4599–4608.

71 X. Lu, H. Hlaing, D. S. Germack, J. Peet, W. H. Jo, D. Andrienko, K. Kremer and B. M. Ocko, Bilayer order in a polycarbazole-conjugated polymer, *Nat. Commun.*, 2012, **3**, 795.

72 C. H. Woo, B. C. Thompson, B. J. Kim, M. F. Toney and J. M. J. Fréchet, The Influence of Poly(3-hexylthiophene) Regioregularity on Fullerene-Composite Solar Cell Performance, *J. Am. Chem. Soc.*, 2008, **130**, 16324–16329.

73 C. Yao, J. Zhao, Y. Zhu, B. Liu, C. Yan, D. F. Perepichka and H. Meng, Trifluoromethyl Group-Modified Non-Fullerene Acceptor toward Improved Power Conversion Efficiency over 13% in Polymer Solar Cells, *ACS Appl. Mater. Interfaces*, 2020, **12**, 11543–11550.

74 L. Zhu, M. Zhang, G. Zhou, T. Hao, J. Xu, J. Wang, C. Qiu, N. Prine, J. Ali, W. Feng, X. Gu, Z. Ma, Z. Tang, H. Zhu, L. Ying, Y. Zhang and F. Liu, Efficient Organic Solar Cell with 16.88% Efficiency Enabled by Refined Acceptor Crystallization and Morphology with Improved Charge Transfer and Transport Properties, *Adv. Energy Mater.*, 2020, **10**, 1904234.

75 H. Lai, Q. Zhao, Z. Chen, H. Chen, P. Chao, Y. Zhu, Y. Lang, N. Zhen, D. Mo, Y. Zhang and F. He, Trifluoromethylation Enables a 3D Interpenetrated Low-Band-Gap Acceptor for Efficient Organic Solar Cells, *Joule*, 2020, **4**, 688–700.

76 W. Wang, C. Yan, T.-K. Lau, J. Wang, K. Liu, Y. Fan, X. Lu and X. Zhan, Fused Hexacyclic Nonfullerene Acceptor with Strong Near-Infrared Absorption for Semitransparent Organic Solar Cells with 9.77% Efficiency, *Adv. Mater.*, 2017, **29**, 1701308.

77 Y.-Q.-Q. Yi, H. Feng, M. Chang, H. Zhang, X. Wan, C. Li and Y. Chen, New small-molecule acceptors based on hexacyclic naphthalene(cyclopentadithiophene) for efficient non-fullerene organic solar cells, *J. Mater. Chem. A*, 2017, **5**, 17204–17210.

78 G. Cai, P. Xue, Z. Chen, T. Li, K. Liu, W. Ma, J. Lian, P. Zeng, Y. Wang, R. P. S. Han and X. Zhan, High-Performance Mid-Bandgap Fused-Pyrene Electron Acceptor, *Chem. Mater.*, 2018, **31**, 6484–6490.

79 C. Huang, X. Liao, K. Gao, L. Zuo, F. Lin, X. Shi, C.-Z. Li, H. Liu, X. Li, F. Liu, Y. Chen, H. Chen and A. K. Y. Jen, Highly Efficient Organic Solar Cells Based on S,N-Heteroacene Non-Fullerene Acceptors, *Chem. Mater.*, 2018, **30**, 5429–5434.

80 J. Wang, J. Zhang, Y. Xiao, T. Xiao, R. Zhu, C. Yan, Y. Fu, G. Lu, X. Lu, S. R. Marder and X. Zhan, Effect of Isomerization on High-Performance Nonfullerene Electron Acceptors, *J. Am. Chem. Soc.*, 2018, **140**, 9140–9147.

81 J.-L. Wang, K.-K. Liu, L. Hong, G.-Y. Ge, C. Zhang and J. Hou, Selenopheno[3,2-*b*]thiophene-Based Narrow-Bandgap Nonfullerene Acceptor Enabling 13.3% Efficiency for Organic Solar Cells with Thickness-Insensitive Feature, *ACS Energy Lett.*, 2018, **3**, 2967–2976.

82 J. Zhu, Z. Ke, Q. Zhang, J. Wang, S. Dai, Y. Wu, Y. Xu, Y. Lin, W. Ma, W. You and X. Zhan, Naphthodithiophene-

Based Nonfullerene Acceptor for High-Performance Organic Photovoltaics: Effect of Extended Conjugation, *Adv. Mater.*, 2018, **30**, 1704713.

83 G. Cai, J. Zhu, Y. Xiao, M. Li, K. Liu, J. Wang, W. Wang, X. Lu, Z. Tang, J. Lian, P. Zeng, Y. Wang and X. Zhan, Fused octacyclic electron acceptor isomers for organic solar cells, *J. Mater. Chem. A*, 2019, **7**, 21432–21437.

84 Y. Wang, B. Liu, C. W. Koh, X. Zhou, H. Sun, J. Yu, K. Yang, H. Wang, Q. Liao, H. Y. Woo and X. Guo, Facile Synthesis of Polycyclic Aromatic Hydrocarbon (PAH)-Based Acceptors with Fine-Tuned Optoelectronic Properties: Toward Efficient Additive-Free Nonfullerene Organic Solar Cells, *Adv. Energy Mater.*, 2019, **9**, 1803976.

85 C. Yao, B. Liu, Y. Zhu, L. Hong, J. Miao, J. Hou, F. He and H. Meng, Highly fluorescent anthracene derivative as a non-fullerene acceptor in OSCs with small non-radiative energy loss of 0.22 eV and high PCEs of over 13%, *J. Mater. Chem. A*, 2019, **7**, 10212–10216.

86 J. Zhao, C. Yao, Y. Zhu, J. Cai, M. U. Ali, J. Miao and H. Meng, Synthesis and characterization of new nonfullerene electron acceptors with a chrysene core, *Dyes Pigm.*, 2020, **174**, 108012.

87 Y. Lin, F. Zhao, Q. He, L. Huo, Y. Wu, T. C. Parker, W. Ma, Y. Sun, C. Wang, D. Zhu, A. J. Heeger, S. R. Marder and X. Zhan, High-Performance Electron Acceptor with Thienyl Side Chains for Organic Photovoltaics, *J. Am. Chem. Soc.*, 2016, **138**, 4955–4961.

88 Y. Yang, Z. G. Zhang, H. Bin, S. Chen, L. Gao, L. Xue, C. Yang and Y. Li, Side-Chain Isomerization on an n-type Organic Semiconductor ITIC Acceptor Makes 11.77% High Efficiency Polymer Solar Cells, *J. Am. Chem. Soc.*, 2016, **138**, 15011–15018.

89 J. Wang, W. Wang, X. Wang, Y. Wu, Q. Zhang, C. Yan, W. Ma, W. You and X. Zhan, Enhancing Performance of Nonfullerene Acceptors via Side-Chain Conjugation Strategy, *Adv. Mater.*, 2017, **29**, 1702125.

90 Y. Lin, F. Zhao, S. K. K. Prasad, J.-D. Chen, W. Cai, Q. Zhang, K. Chen, Y. Wu, W. Ma, F. Gao, J.-X. Tang, C. Wang, W. You, J. M. Hodgkiss and X. Zhan, Balanced Partnership between Donor and Acceptor Components in Nonfullerene Organic Solar Cells with >12% Efficiency, *Adv. Mater.*, 2018, **30**, 1706363.

91 S. Li, L. Ye, W. Zhao, S. Zhang, S. Mukherjee, H. Ade and J. Hou, Energy-Level Modulation of Small-Molecule Electron Acceptors to Achieve over 12% Efficiency in Polymer Solar Cells, *Adv. Mater.*, 2016, **28**, 9423–9429.

92 S. Dai, F. Zhao, Q. Zhang, T. K. Lau, T. Li, K. Liu, Q. Ling, C. Wang, X. Lu, W. You and X. Zhan, Fused Nonacyclic Electron Acceptors for Efficient Polymer Solar Cells, *J. Am. Chem. Soc.*, 2017, **139**, 1336–1343.

93 S. Li, L. Ye, W. Zhao, X. Liu, J. Zhu, H. Ade and J. Hou, Design of a New Small-Molecule Electron Acceptor Enables Efficient Polymer Solar Cells with High Fill Factor, *Adv. Mater.*, 2017, **29**, 1704051.

94 S. Li, L. Ye, W. Zhao, S. Zhang, H. Ade and J. Hou, Significant Influence of the Methoxyl Substitution Position on Optoelectronic Properties and Molecular Packing of Small-Molecule Electron Acceptors for Photovoltaic Cells, *Adv. Energy Mater.*, 2017, **7**, 1700183.

95 H. Yao, L. Ye, J. Hou, B. Jang, G. Han, Y. Cui, G. M. Su, C. Wang, B. Gao, R. Yu, H. Zhang, Y. Yi, H. Y. Woo, H. Ade and J. Hou, Achieving Highly Efficient Nonfullerene Organic Solar Cells with Improved Intermolecular Interaction and Open-Circuit Voltage, *Adv. Mater.*, 2017, **29**, 1700254.

96 S. S. Wan, C. Chang, J. L. Wang, G. Z. Yuan, Q. Wu, M. Zhang and Y. Li, Effects of the Number of Bromine Substitution on Photovoltaic Efficiency and Energy Loss of Benzo[1,2-*b*:4,5-*b*′]diselenophene-based Narrow-Bandgap Multibrominated Nonfullerene Acceptors, *Sol. RRL*, 2019, **3**, 1800250.

97 N. B. Kolhe, S. M. West, D. K. Tran, X. Ding, D. Kuzuhara, N. Yoshimoto, T. Koganezawa and S. A. Jenekhe, Designing High Performance Nonfullerene Electron Acceptors with Rylene Imides for Efficient Organic Photovoltaics, *Chem. Mater.*, 2019, **32**, 195–204.

98 J. Qu, D. Li, H. Wang, J. Zhou, N. Zheng, H. Lai, T. Liu, Z. Xie and F. He, Bromination of the Small-Molecule Acceptor with Fixed Position for High-Performance Solar Cells, *Chem. Mater.*, 2019, **31**, 8044–8051.

99 L. Feng, J. Yuan, Z. Zhang, H. Peng, Z.-G. Zhang, S. Xu, Y. Liu, Y. Li and Y. Zou, Thieno[3,2-b]pyrrolo-Fused Pentacyclic Benzotriazole-Based Acceptor for Efficient Organic Photovoltaics, *ACS Appl. Mater. Interfaces*, 2017, **9**, 31985–31992.

100 J. Yuan, T. Huang, P. Cheng, Y. Zou, H. Zhang, J. L. Yang, S. Y. Chang, Z. Zhang, W. Huang, R. Wang, D. Meng, F. Gao and Y. Yang, Enabling low voltage losses and high photocurrent in fullerene-free organic photovoltaics, *Nat. Commun.*, 2019, **10**, 570.

101 M. Luo, L. Zhou, J. Yuan, C. Zhu, F. Cai, J. Hai and Y. Zou, A new non-fullerene acceptor based on the heptacyclic benzotriazole unit for efficient organic solar cells, *J. Energy Chem.*, 2020, **42**, 169–173.

102 Y. Zhang, F. Cai, J. Yuan, Q. Wei, L. Zhou, B. Qiu, Y. Hu, Y. Li, H. Peng and Y. Zou, A new non-fullerene acceptor based on the combination of a heptacyclic benzothiadiazole unit and a thiophene-fused end group achieving over 13% efficiency, *Phys. Chem. Chem. Phys.*, 2019, **21**, 26557–26563.

103 S. Liu, J. Yuan, W. Deng, M. Luo, Y. Xie, Q. Liang, Y. Zou, Z. He, H. Wu and Y. Cao, High-efficiency organic solar cells with low non-radiative recombination loss and low energetic disorder, *Nat. Photonics*, 2020, **14**, 300–305.

104 M. Luo, C. Zhao, J. Yuan, J. Hai, F. Cai, Y. Hu, H. Peng, Y. Bai, Z. A. Tan and Y. Zou, Semitransparent solar cells with over 12% efficiency based on a new low bandgap fluorinated small molecule acceptor, *Mater. Chem. Front.*, 2019, **3**, 2483–2490.

105 M. Luo, C. Zhu, J. Yuan, L. Zhou, M. L. Keshtov, D. Y. Godovsky and Y. Zou, A chlorinated non-fullerene acceptor for efficient polymer solar cells, *Chin. Chem. Lett.*, 2019, **30**, 2343–2346.

106 Z. Zhou, W. Liu, G. Zhou, M. Zhang, D. Qian, J. Zhang, S. Chen, S. Xu, C. Yang, F. Gao, H. Zhu, F. Liu and X. Zhu, Subtle Molecular Tailoring Induces Significant Morphology Optimization Enabling over 16% Efficiency Organic Solar Cells with Efficient Charge Generation, *Adv. Mater.*, 2020, **32**, 1906324.

107 B. Fan, D. Zhang, M. Li, W. Zhong, Z. Zeng, L. Ying, F. Huang and Y. Cao, Achieving over 16% efficiency for single-junction organic solar cells, *Sci. China: Chem.*, 2019, **62**, 746–752.

108 J. Xiao, T. Yan, T. Lei, Y. Li, Y. Han, L. cao, W. Song, S. Tan and Z. Ge, Organic solar cells based on non-fullerene acceptors of nine fused-ring by modifying end groups, *Org. Electron.*, 2020, **81**, 105662.

109 K. Jiang, Q. Wei, J. Y. L. Lai, Z. Peng, H. K. Kim, J. Yuan, L. Ye, H. Ade, Y. Zou and H. Yan, Alkyl Chain Tuning of Small Molecule Acceptors for Efficient Organic Solar Cells, *Joule*, 2019, **3**, 3020–3033.

110 L. Hong, H. Yao, Z. Wu, Y. Cui, T. Zhang, Y. Xu, R. Yu, Q. Liao, B. Gao, K. Xian, H. Y. Woo, Z. Ge and J. Hou, Eco-Compatible Solvent-Processed Organic Photovoltaic Cells with Over 16% Efficiency, *Adv. Mater.*, 2019, **31**, 1903441.

111 Y. Cui, H. Yao, L. Hong, T. Zhang, Y. Tang, B. Lin, K. Xian, B. Gao, C. An, P. Bi, W. Ma and J. Hou, 17% Efficiency Organic Photovoltaic Cell with Superior Processability, *Natl. Sci. Rev.*, 2019, DOI: 10.1093/nsr/nwz200.

112 Y. Cui, H. Yao, J. Zhang, K. Xian, T. Zhang, L. Hong, Y. Wang, Y. Xu, K. Ma, C. An, C. He, Z. Wei, F. Gao and J. Hou, Single-Junction Organic Photovoltaic Cells with Approaching 18% Efficiency, *Adv. Mater.*, 2020, **32**, 1908205.

113 J. Yuan, Y. Zhang, L. Zhou, C. Zhang, T. K. Lau, G. Zhang, X. Lu, H. L. Yip, S. K. So, S. Beaupré, M. Mainville, P. A. Johnson, M. Leclerc, H. Chen, H. Peng, Y. Li and Y. Zou, Fused Benzothiadiazole: A Building Block for n-Type Organic Acceptor to Achieve High-Performance Organic Solar Cells, *Adv. Mater.*, 2019, **31**, 1807577.

114 R. Wang, J. Yuan, R. Wang, G. Han, T. Huang, W. Huang, J. Xue, H. C. Wang, C. Zhang, C. Zhu, P. Cheng, D. Meng, Y. Yi, K. H. Wei, Y. Zou and Y. Yang, Rational Tuning of Molecular Interaction and Energy Level Alignment Enables High-Performance Organic Photovoltaics, *Adv. Mater.*, 2019, **31**, 1904215.

115 Y. Cui, H. Yao, J. Zhang, T. Zhang, Y. Wang, L. Hong, K. Xian, B. Xu, S. Zhang, J. Peng, Z. Wei, F. Gao and J. Hou, Over 16% efficiency organic photovoltaic cells enabled by a chlorinated acceptor with increased open-circuit voltages, *Nat. Commun.*, 2019, **10**, 2515.

116 H. Wang, T. Liu, J. Zhou, D. Mo, L. Han, H. Lai, H. Chen, N. Zheng, Y. Zhu, Z. Xie and F. He, Bromination: An Alternative Strategy for Non-Fullerene Small Molecule Acceptors, *Adv. Sci.*, 2020, **7**, 1903784.

117 R. Qin, D. Wang, G. Zhou, Z.-P. Yu, S. Li, Y. Li, Z.-X. Liu, H. Zhu, M. Shi, X. Lu, C.-Z. Li and H. Chen, Tuning terminal aromatics of electron acceptors to achieve high-efficiency organic solar cells, *J. Mater. Chem. A*, 2019, **7**, 27632–27639.

118 W. Yang, Z. Luo, R. Sun, J. Guo, T. Wang, Y. Wu, W. Wang, J. Guo, Q. Wu, M. Shi, H. Li, C. Yang and J. Min, Simultaneous enhanced efficiency and thermal stability in organic solar cells from a polymer acceptor additive, *Nat. Commun.*, 2020, **11**, 1218.

119 X. Ma, M. Luo, W. Gao, J. Yuan, Q. An, M. Zhang, Z. Hu, J. Gao, J. Wang, Y. Zou, C. Yang and F. Zhang, Achieving 14.11% efficiency of ternary polymer solar cells by simultaneously optimizing photon harvesting and exciton distribution, *J. Mater. Chem. A*, 2019, **7**, 7843–7851.

120 L. Zhan, S. Li, T.-K. Lau, Y. Cui, X. Lu, M. Shi, C.-Z. Li, H. Li, J. Hou and H. Chen, Over 17% efficiency ternary organic solar cells enabled by two non-fullerene acceptors working in an alloy-like model, *Energy Environ. Sci.*, 2020, **13**, 635–645.

121 J. Gao, W. Gao, X. Ma, Z. Hu, C. Xu, X. Wang, Q. An, C. Yang, X. Zhang and F. Zhang, Over 14.5% efficiency and 71.6% fill factor of ternary organic solar cells with 300 nm thick active layers, *Energy Environ. Sci.*, 2020, **13**, 958–967.

122 A. Balan, D. Baran and L. Toppare, Benzotriazole containing conjugated polymers for multipurpose organic electronic applications, *Polym. Chem.*, 2011, **2**, 1029–1043.

123 T. Khanasa, N. Prachumrak, R. Rattanawan, S. Jungsuttiwong, T. Keawin, T. Sudyoadsuk, T. Tuntulani and V. Promarak, An efficient solution processed non-doped red emitter based on carbazole-triphenylamine end-capped di(thiophen-2-yl)benzothiadiazole for pure red organic light-emitting diodes, *Chem. Commun.*, 2013, **49**, 3401–3403.

124 I. Meager, M. Nikolka, B. C. Schroeder, C. B. Nielsen, M. Planells, H. Bronstein, J. W. Rumer, D. I. James, R. S. Ashraf, A. Sadhanala, P. Hayoz, J.-C. Flores, H. Sirringhaus and I. McCulloch, Thieno[3,2-*b*]thiophene Flanked Isoindigo Polymers for High Performance Ambipolar OFET Applications, *Adv. Funct. Mater.*, 2014, **24**, 1402307.

125 W. Li, Y. Guo, J. Shi, H. Yu and H. Meng, Solution-Processable Neutral Green Electrochromic Polymer Containing Thieno[3,2-*b*]thiophene Derivative as Unconventional Donor Units, *Macromolecules*, 2016, **49**, 7211–7219.

126 W. Li, J. Ning, Y. Yin, X. Xing, M. Qi, T. Li, J. Cao, Y. He, I. F. Perepichka and H. Meng, Thieno[3,2-*b*]thiophene-based conjugated copolymers for solution-processable neutral black electrochromism, *Polym. Chem.*, 2018, **9**, 5608–5616.

127 S. C. Price, A. C. Stuart, L. Yang, H. Zhou and W. You, Fluorine Substituted Conjugated Polymer of Medium Band Gap Yields 7% Efficiency in Polymer−Fullerene Solar Cells, *J. Am. Chem. Soc.*, 2011, **133**, 4625–4631.

128 Q. Fan, W. Su, X. Meng, X. Guo, G. Li, W. Ma, M. Zhang and Y. Li, High-Performance Non-Fullerene Polymer Solar Cells Based on Fluorine Substituted Wide Bandgap Copolymers Without Extra Treatments, *Sol. RRL*, 2017, **1**, 1700020.

129 H. Huang, H. Bin, Z. Peng, B. Qiu, C. Sun, A. Liebman-Pelaez, Z.-G. Zhang, C. Zhu, H. Ade, Z. Zhang and Y. Li, Effect of Side-Chain Engineering of Bithienylbenzodithiophene-*alt*-fluorobenzotriazole-Based Copolymers on the

Thermal Stability and Photovoltaic Performance of Polymer Solar Cells, *Macromolecules*, 2018, **51**, 6028–6036.

130 T. Yan, H. Bin, C. Sun, Z. G. Zhang and Y. Li, Effect of Thieno[3,2-*b*]thiophene π-bridge on photovoltaic performance of a D–A copolymer of alkoxy-benzodithiophene-*alt*-fluoro-benzotriazole, *Org. Electron.*, 2018, **55**, 106–111.

131 J. Yu, P. Chen, C. W. Koh, H. Wang, K. Yang, X. Zhou, B. Liu, Q. Liao, J. Chen, H. Sun, H. Y. Woo, S. Zhang and X. Guo, Polymer Semiconductors: Phthalimide-Based High Mobility Polymer Semiconductors for Efficient Nonfullerene Solar Cells with Power Conversion Efficiencies over 13%, *Adv. Sci.*, 2019, **6**, 1970012.

132 S. Holliday, R. S. Ashraf, A. Wadsworth, D. Baran, S. A. Yousaf, C. B. Nielsen, C. H. Tan, S. D. Dimitrov, Z. Shang, N. Gasparini, M. Alamoudi, F. Laquai, C. J. Brabec, A. Salleo, J. R. Durrant and I. McCulloch, High-efficiency and air-stable P3HT-based polymer solar cells with a new non-fullerene acceptor, *Nat. Commun.*, 2016, **7**, 11585.

133 S. Holliday, R. S. Ashraf, C. B. Nielsen, M. Kirkus, J. A. Röhr, C.-H. Tan, E. Collado-Fregoso, A.-C. Knall, J. R. Durrant, J. Nelson and I. McCulloch, A Rhodanine Flanked Non-fullerene Acceptor for Solution-Processed Organic Photovoltaics, *J. Am. Chem. Soc.*, 2015, **137**, 898–904.

134 J. Miao, B. Meng, J. Liu and L. Wang, An A–D–A′–D–A type small molecule acceptor with a broad absorption spectrum for organic solar cells, *Chem. Commun.*, 2018, **54**, 303–306.

135 D. Mo, H. Chen, J. Zhou, N. Tang, L. Han, Y. Zhu, P. Chao, H. Lai, Z. Xie and F. He, Alkyl chain engineering of chlorinated acceptors for elevated solar conversion, *J. Mater. Chem. A*, 2020, **8**, 8903–8912.

136 Y. Lin, B. Adilbekova, Y. Firdaus, E. Yengel, H. Faber, M. Sajjad, X. Zheng, E. Yarali, A. Seitkhan, O. M. Bakr, A. El-Labban, U. Schwingenschlögl, V. Tung, I. McCulloch, F. Laquai and T. D. Anthopoulos, 17% Efficient Organic Solar Cells Based on Liquid Exfoliated WS2 as a Replacement for PEDOT:PSS, *Adv. Mater.*, 2019, **31**, 1902965.

137 Q. Yang, S. Yu, P. Fu, W. Yu, Y. Liu, X. Liu, Z. Feng, X. Guo and C. Li, Boosting Performance of Non-Fullerene Organic Solar Cells by 2D g-C_3N_4 Doped PEDOT:PSS, *Adv. Funct. Mater.*, 2020, **30**, 1910205.

138 L. Perdigon-Toro, H. Zhang, A. Markina, J. Yuan, S. M. Hosseini, C. M. Wolff, G. Zuo, M. Stolterfoht, Y. Zou, F. Gao, D. Andrienko, S. Shoaee and D. Neher, Barrierless Free Charge Generation in the High-Performance PM6:Y6 Bulk Heterojunction Non-Fullerene Solar Cell, *Adv. Mater.*, 2020, **32**, 1906763.

139 L. Yang, L. Yan and W. You, Organic Solar Cells beyond One Pair of Donor–Acceptor: Ternary Blends and More, *J. Phys. Chem. Lett.*, 2013, **4**, 1802–1810.

140 M.-A. Pan, T.-K. Lau, Y. Tang, Y.-C. Wu, T. Liu, K. Li, M.-C. Chen, X. Lu, W. Ma and C. Zhan, 16.7%-efficiency ternary blended organic photovoltaic cells with PCBM as the acceptor additive to increase the open-circuit voltage and phase purity, *J. Mater. Chem. A*, 2019, **7**, 20713–20722.

141 T. Yan, W. Song, J. Huang, R. Peng, L. Huang and Z. Ge, 16.67% Rigid and 14.06% Flexible Organic Solar Cells Enabled by Ternary Heterojunction Strategy, *Adv. Mater.*, 2019, **31**, 1902210.

142 R. Yu, H. Yao, Y. Cui, L. Hong, C. He and J. Hou, Improved Charge Transport and Reduced Nonradiative Energy Loss Enable Over 16% Efficiency in Ternary Polymer Solar Cells, *Adv. Mater.*, 2019, **31**, 1902302.

143 J. Song, C. Li, L. Zhu, J. Guo, J. Xu, X. Zhang, K. Weng, K. Zhang, J. Min, X. Hao, Y. Zhang, F. Liu and Y. Sun, Ternary Organic Solar Cells with Efficiency >16.5% Based on Two Compatible Nonfullerene Acceptors, *Adv. Mater.*, 2019, **31**, 1905645.

144 N. Gasparini, S. H. K. Paleti, J. Bertrandie, G. Cai, G. Zhang, A. Wadsworth, X. Lu, H.-L. Yip, I. McCulloch and D. Baran, Exploiting Ternary Blends for Improved Photostability in High-Efficiency Organic Solar Cells, *ACS Energy Lett.*, 2020, **5**, 1371–1379.

145 K. Li, Y. Wu, Y. Tang, M. A. Pan, W. Ma, H. Fu, C. Zhan and J. Yao, Ternary Blended Fullerene-Free Polymer Solar Cells with 16.5% Efficiency Enabled with a Higher-LUMO-Level Acceptor to Improve Film Morphology, *Adv. Energy Mater.*, 2019, **9**, 1901728.

146 H. W. Cheng, H. Zhang, Y. C. Lin, N. Z. She, R. Wang, C. H. Chen, J. Yuan, C. S. Tsao, A. Yabushita, Y. Zou, F. Gao, P. Cheng, K. H. Wei and Y. Yang, Realizing Efficient Charge/Energy Transfer and Charge Extraction in Fullerene-Free Organic Photovoltaics via a Versatile Third Component, *Nano Lett.*, 2019, **19**, 5053–5061.

147 X. Xu, K. Feng, Z. Bi, W. Ma, G. Zhang and Q. Peng, Single-Junction Polymer Solar Cells with 16.35% Efficiency Enabled by a Platinum(II) Complexation Strategy, *Adv. Mater.*, 2019, **31**, 1901872.

148 H. Sun, T. Liu, J. Yu, T.-K. Lau, G. Zhang, Y. Zhang, M. Su, Y. Tang, R. Ma, B. Liu, J. Liang, K. Feng, X. Lu, X. Guo, F. Gao and H. Yan, A monothiophene unit incorporating both fluoro and ester substitution enabling high-performance donor polymers for non-fullerene solar cells with 16.4% efficiency, *Energy Environ. Sci.*, 2019, **12**, 3328–3337.

149 J. Xiong, K. Jin, Y. Jiang, J. Qin, T. Wang, J. Liu, Q. Liu, H. Peng, X. Li, A. Sun, X. Meng, L. Zhang, L. Liu, W. Li, Z. Fang, X. Jia, Z. Xiao, Y. Feng, X. Zhang, K. Sun, S. Yang, S. Shi and L. Ding, Thiolactone copolymer donor gifts organic solar cells a 16.72% efficiency, *Sci. Bull.*, 2019, **64**, 1573–1576.

